INVESTIGATION OF THE FLOW OF THE UPPER PLENUM OF A SCALED VERY HIGH TEMPERATURE REACTOR DURING A DEPRESSURIZED COOLDOWN CONDUCTION ACCIDENT

A Thesis

by

ANAS MOHAMMED F ALWAFI

Submitted to the Office of Graduate and Professional Studies of
Texas A&M University
in partial fulfillment of the requirements for the degree of

MASTER OF SCIENCE

Chair of Committee,	Yassin A. Hassan
Committee Members,	William H. Marlow
	Maria D. King
Head of Department,	Yassin A. Hassan

December 2015

Major Subject: Nuclear Engineering

ABSTRACT

Very High Temperature Reactors (VHTRs) are the future of nuclear reactors. A 1/16th scaled upper plenum of a VHTR was designed and assembled at Texas A&M University (TAMU) in order to study the behavior of flow in the upper plenum of a VHTR. Flow was investigated under one major accident scenario, the Depressurized Conduction Cooldown (DCC); this occurs due to loss of force when operation is interrupted by loss of power. In this case, the fluid will have a natural convection, forcing it to flow to the upper plenum. Particle Tracking Velocimetry (PTV) was used to illustrate flow, using water as the working fluid. A PTV code was used to track the particles, and this was then averaged over all vectors after filtering out those that failed. All flow velocity compounds, such as the velocity magnitude, y-velocity, x-velocity, standard deviation, and flow streamlines were visualized. A sensitivity analysis was performed in order to confirm that the number of frames used was sufficient to reach a steady state. In addition, repeatability analysis was applied to the output data. Turbulent intensity, Reynolds stress, and error occurring with these tests were all estimated. Finally, experimental data was validated using benchmark data.

DEDICATION

This thesis is dedicated to who always encouraged me to seek knowledge by repeating: “Son: Ask for knowledge, even by swimming.” my father, who just passed away two years ago while I was still at the beginning of my graduate studies; his words and wisdom have always inspired me to work hard. Father I wish you can see me now!

To my lovely mom, Amina, who spent her life sacrificing herself for me. Her hopes for my success and her unlimited support always encouraged me to achieve my goals. I will never forget all that she did for me.

To Sarah, my soul mate and wife, who is always supporting and encouraging me. She never stopped me in my path. Instead, she made the choice to accompany me to the United States. Her patience and endless love have helped me get past all of the stressful moments.

To my three-year-old baby, Omar. His smile keeps me working hard for him and his future siblings.

To my brothers AbdullElah, Osama, Yousef, and Albaraa, my sisters Asmah, Somyah, Enas, and Jooo and my sisters' husbands Tawafeeq and Ramzi.

I am honored to dedicate this work to all of you. Thank you for your support and unlimited prayers.

ACKNOWLEDGEMENTS

First, I would like to thank my advisor, Dr. Yassin Hassan. It was such a great experience to work under him. I would like to highlight how his visits to the lab, his guidance, and his sharing of his experience have encouraged me to approach my studies professionally.

I would like to express my thanks to Dr. N. K. Anand from the mechanical engineering department; his Saturday meetings were invaluable to me and to the project.

I also want to thank my committee members, Dr. William Marlow and Dr. Maria King for their support.

My special acknowledgment and thanks go to my colleague and friend, Robert Park, a PhD candidate with whom I worked on the same project and shared the same office. His endless help and time were the keys to the success of this study. Sometimes, he spent all night teaching me how to run the code and he explained the physical meaning of a graph to me as well.

I would also like to acknowledge Dr. Saya Lee and Dr. Calrose Esrada-Perez. Despite their busy schedules, they did not hesitate to take the time to give me advice when I needed it.

I would like to thank my father-in-law, Mr. Abdulrahman Alyousef. I consider this man my father as he took care of me after the death of my own. I can always count on him when I need advice. Special thanks are also extended to my mother-in-law, Hajer, and my brothers-in-law, Yousef, Abdulaziz, and Abdullah, and my sister-in-law, Nouf.

I would like to express my thanks to my best friends, Abdulla Alnaqeep and Mohammed Bajhaln. They support me all the time. If I need to talk about my problems, they are always my first choice.

In addition, I would like to acknowledge my sponsor, King Abdulaziz City for Science and Technology (KACST), for the opportunity that was given to me to study at one of the finest universities in the world. Especially my former supervisor, Dr. Khalid Alesa. His confidence in me has been extremely valuable to the completion of this piece of work.

Finally, I would like to thank the Saudi Arabian Cultural Mission (SACM) in the USA for the services that they provided to make it easier for me to carry out my studies.

TABLE OF CONTENTS

Page

LIST OF FIGURES

Page

LIST OF TABLES

Page

CHAPTER I

INTRODUCTION

Energy demand is currently a big concern for world leaders. By 2040, global energy demand is projected to grow by 37% [1]. Nuclear power plants are one of the advancements in technology that can supply this energy demand. Approximately 11% of the world's electricity is produced by 435 nuclear power reactors operating in 31 countries. Moreover, there are approximately 70 reactors presently under construction, including emerging nuclear energy countries such as the United Arab Emirates (UAE) [2]. Countries such as Saudi Arabia, Jordan, Turkey and Vietnam have either signed a contract, or committed to a plan, to build their first nuclear power plan. Thus, nuclear power seems likely to play an important role for the future supply of energy worldwide. At present, most nuclear reactors in use Generation II reactors, either Boiling Water Reactors (BWR) or Pressurized Water Reactors (PWR). In BWR, the reactor heats the water to boiling, and then the steam goes to the turbine [3]. On the other hand, PWRs heat water, which then gets pressurized before the steam goes to the turbine [4]. At the same time, nuclear reactor technology is still under development, and generation III reactors, or Advanced Boiling Water Reactors (ABWR), operate with higher quality. These reactors work similarly to a BWR, but with higher efficiency and less space requirements [5]. Generation IV is the future of nuclear reactors and is safer and more economical than the older generations [6]. (Figure 1) illustrates the five generations of the reactors.

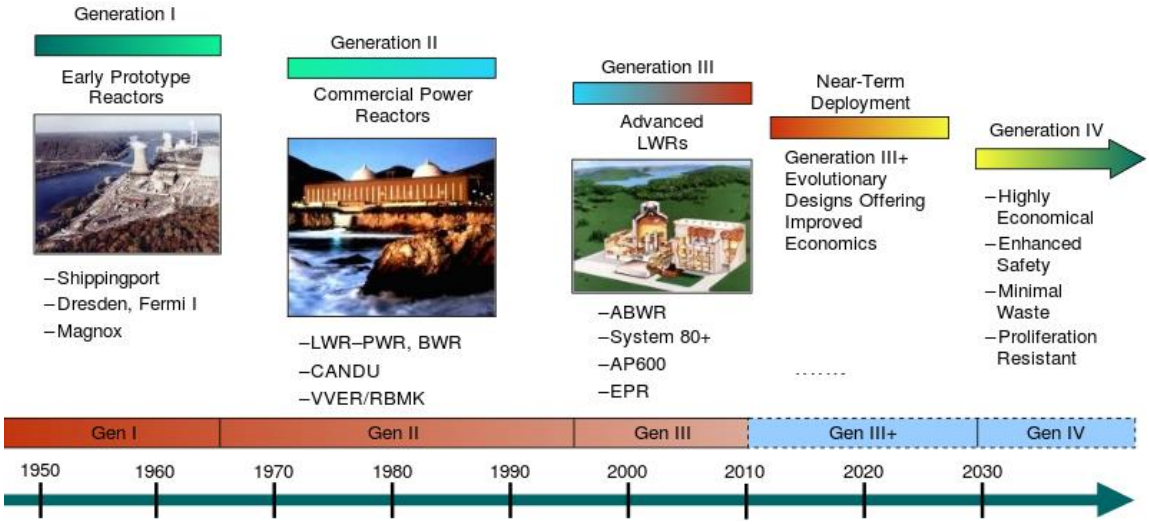

Figure 1. Generations of nuclear technology

I.1. Project Background

One of the most promising reactors in Generation IV is the Very High Temperature Reactor (VHTR). Its core outlet temperature reaches1000℃ or higher, allowing it to generate more energy. It uses helium gas as a coolant and graphite as a moderator. It will be designed with more than 50% efficiency and a thermal power between 600 and 800 MWth. The coated fuel will use a low uranium fuel with high burn-up. Also, it will be an environmentally-friendly reactor as shown in Figure 2 [7]. In 2002, the U.S. Nuclear Energy Research Advisory Committee (NERAC) and the Generation IV International Forum (GIF) proved that the VHTR is more sustainable, economical, safe and reliable than any other kind of reactor, with superior proliferation resistance and physical protection [8]. Besides its main application for energy production, VHTR will

be valuable for other industrial applications, since VHTR uses an indirect cycle in the heat exchanger. For example, industrial applications such as iron and glass manufacturing require temperatures of more than 800 ℃ for processing and using VHTR for this application will reduce the cost of manufacturing [7]. Using VHTR for all of these applications will thus help to reduce the emission of greenhouse gases.

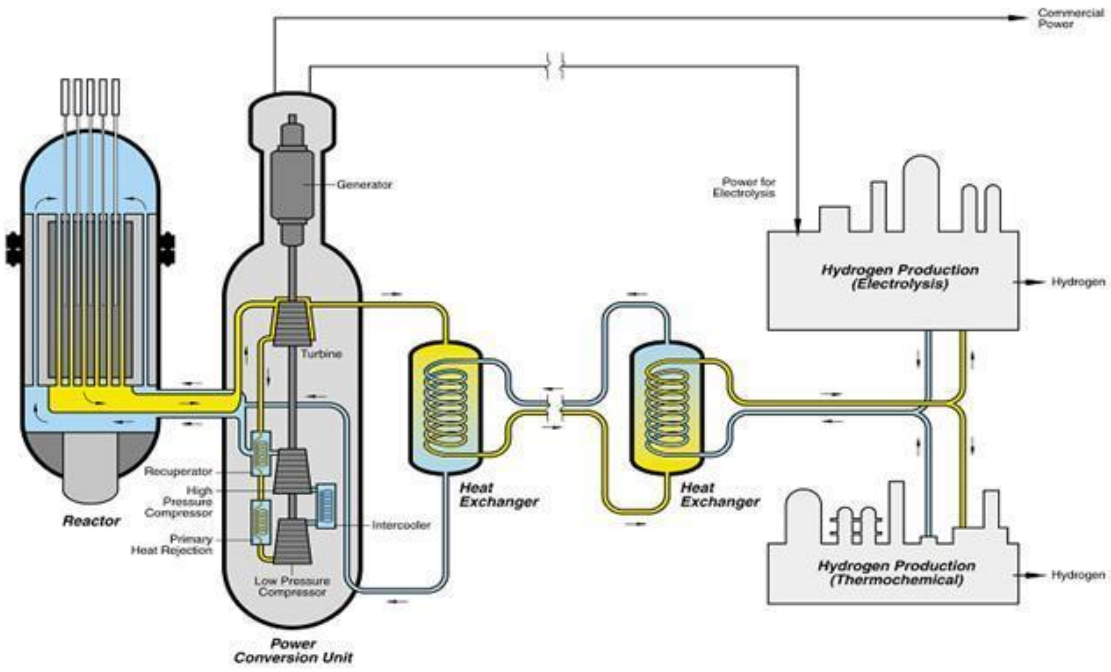

Figure 2. Schematic of the very high temperature reactor.

Given that the VHTR is cutting-edge technology, investigating its safety is key to ensuring its success. The Department of Energy (DOE) and the Idaho National Lab (INL) are developing a safety code for the reactor to be used under normal operations and in the case of an accident. Two main accident scenarios can occur with VHTRs: the Depressurized Conduction Cooldown (DCC), and the Pressurized Conduction Cooldown (PCC). Under normal operation, a pump is used to add coolant to the reflector and the core, and then goes up to the upper plenum and returns down to the heat exchanger (Figure 3 illustrates the operation).

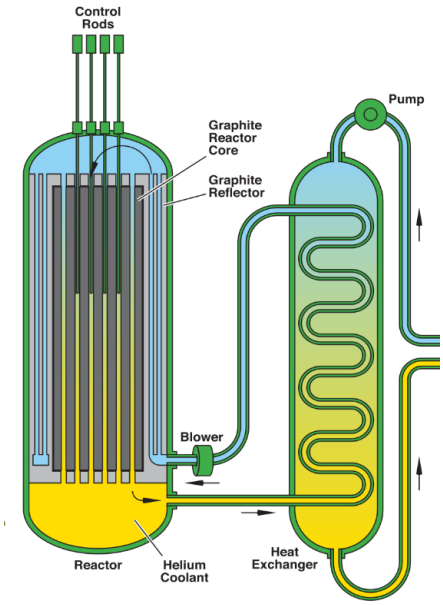

Figure 3. VHTR under normal operation.

PCC accidents occur when there is a loss of force during reactor scram as a result of loss of power. During reactor scram, all blowers and pumps cease working, but the primary system remains at full pressure. Here, natural convection will move the heat from the core to the reactor cavity cooling system (RCCS). DCC accidents result from the cooling loop depressurizing, thus the reactor scram occurs due to loss of power and loss of pressure in the primary system [9].

I.2. Objectives

The main scope of the current research is to study the flow at the upper plenum of a VHTR under a DCC accident scenario. A test facility designed and constructed at Texas A&M University was used to test a $1/16^{th}$ VHTR model that simulates the upper plenum of the VHTR. The experimental facility is capable of providing data on the flow in the upper plenum of the VHTR under different accident scenarios. These data also provide reliable support for Computational Fluid Dynamics (CFD) analysis. There are several methods with which to investigate flow in any particular area of the system can be investigated by several methods; here, I use Particle Tracking Velocimetry (PTV) to measure velocity at the upper plenum.

I.3. Outline

This chapter covers the background and the objective for this research. The main focus is on VHTR and its applications. In addition, different scenario accidents were described.

Chapter II provides a literature review. It covers studies done to design a $1/16^{th}$ scaled upper plenum of a VHTR at TAMU, which was provided by the Idaho National lab (INL). Different model scaling and analysis are covered, such as a High Temperature Test Facility (HTTF) at Oregon State University. Then, particle image velocimetry (PIV), and Particle Tracking Velocimetry (PTV) techniques are covered in detail. Both techniques are used to analyze flow.

Chapter III gives detailed information about the test facility used in the current study. Each component is discussed, including any problems that arose during assembly and how they were fixed. In addition, the instruments used in the test facility are described.

Chapter IV covers the test procedure. The PTV code and its algorithm are explained. The output data are presented as a tecplot. Sensitivity analysis was done to determine how many image frames are sufficient to achieve a steady state. Finally, data were validated using benchmark data.

Chapter V provides conclusions arising from the experimental work and suggests some future work.

CHAPTER II

LITERATURE REVIEW

II.1. Modeling

Idaho National lab (INL) has been investing the scaling and modeling of VHTRs. At the 2015 International Conference on Nuclear Energy (ICONE 15), McCreery, Condie, and Schultz presented a paper on this topic, [10] covering the basic design and methods for the scaling. The scaling approach was created to match the Reynolds number, the ratio of inertial force to viscous forces, to the Richardson number, the ratio of buoyant to inertial forces.

As temperature changes in the system, the Boussinesq approximation is used to solve density:

$$\rho = \rho_0 + \Delta\rho \tag{II.1a}$$

and combined with the Navier-Stokes equation [11] to solve for change in velocity:

$$\frac{D\bar{V}}{Dt} = -\frac{\nabla P}{\rho} + v\nabla^2\bar{V} + \frac{\Delta\rho}{\rho}\bar{g} \tag{II.1b}$$

where, ρ is the density, $\bar{V}$ is the velocity vector, t is time, P is pressure, v is kinematic velocity and $\bar{g}$ is the gravity force.

Due to the change of density with the change of temperature, it can be solved as:

$$\Delta\rho = -\alpha\rho_0\Delta T \tag{II.2}$$

where, α is the thermal expansion coefficient.

Using the definition of the Richardson number:

$$R_i = \frac{g\left(\frac{\Delta T}{T}\right)D}{V^2} \tag{II.3}$$

$$\frac{Re_m}{Re_p} = \frac{\left(\frac{\Delta\rho}{\rho}\right)_m}{\left(\frac{\Delta\rho}{\rho}\right)_p}\frac{V_p^2}{V_m^2}\frac{D_m}{D_p} \tag{II.4}$$

If the Richardson number matches the model and the prototype, then the Reynolds number ratio may be expressed as:

$$\frac{Re_m}{Re_p} = \left[\frac{\left(\frac{\Delta\rho}{\rho}\right)_m}{\left(\frac{\Delta\rho}{\rho}\right)_p}\right]^{1/2}\left[\frac{D_m}{D_p}\right]^{3/2}\frac{v_p}{v_m} \tag{II.5}$$

Based on this INL work, Oregon State University simulated a model using a 1/4 scaled VHTR at their High Temperature Test Facility (HTTF). They studied the flow in the upper and lower plenum for natural convection, DCC and PCC accidents scenarios.

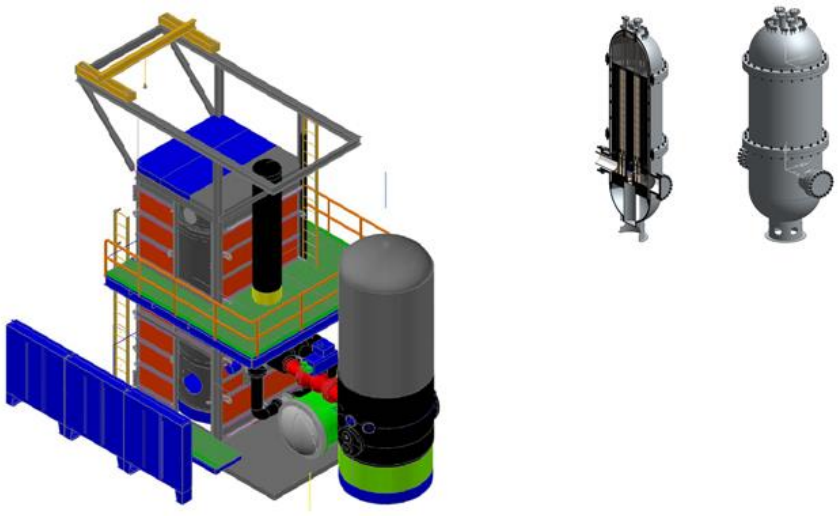

Figure 4. Oregon State University's high temperature test facility.

Results from their study provided information on phenomena that occurred and allowed them to build a safety and analysis code for the VHTR [12]. The HTTF vessel is scaled down to be 6.1 m long with a diameter of 1.92 m. It is made of stainless steel, with ceramic in the upper and lower heads. The pressure is approximately 8 bar. Table 1 gives an overview of the ratio of HTTF [13].

Table 1. Scaling ratios for HTTF.

Parameter	Ratio
Length	1:4
Diameter	1:7.54
Area	1:56.85
Volume	1:227.4
Velocity	1:2
Power	1:113.7
Power Density	2:1
Flow Resistance	1:1
Pressure Drop	1:4
Time	1:2

More recently, the nuclear engineering department at Texas A&M University designed and built a 1/16th-scaled experimental facility that simulates the upper plenum of the VHTR. They used the same procedure as HTTF to scale down the VHTR. However, TAMU's test facility was designed only for the upper plenum of VHTR and uses water instant of helium. Because the TAMU test facility operates at a lower temperature and pressure than the prototype, the Reynold's number and Richardson number do not match with helium. Water, on the other hand, has the property to match

Reynolds and Richardson numbers. This was a preliminary study for the design. The aim of the study was to test the Particle Image Velocimetry (PIV) system to investigate flow, and it is further capable of generating more experimental data for the upper plenum in different accident scenarios. Table 2 and Figure 5 illustrate the dimensions of a 1/16th scaled TAMU test facility [14].

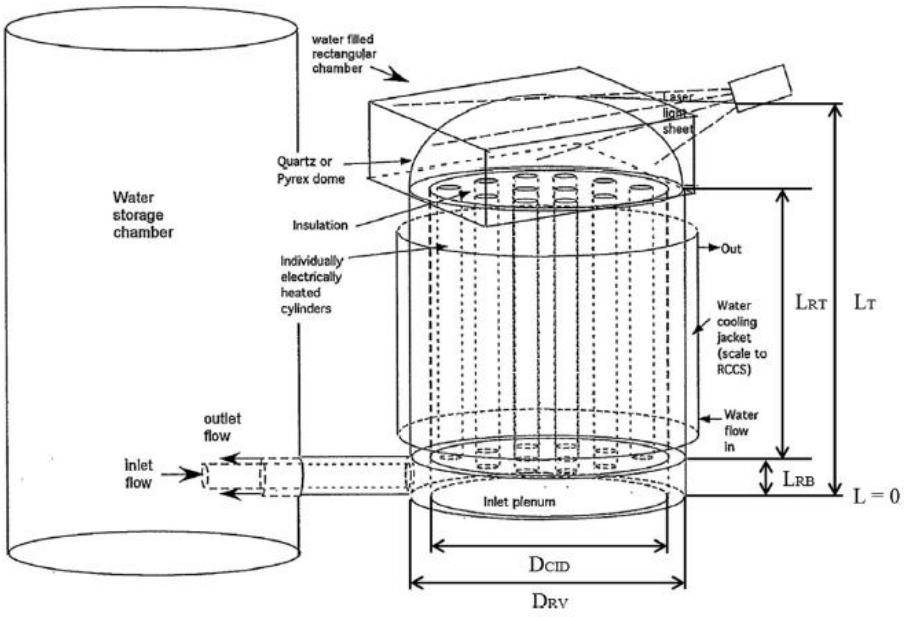

Figure 5. Design of Texas A&M University test facility of a 1/16th scaled VHTR.

Table 2. Dimensions of MHTGR and a 1/16th scaled VHTR.

Dimension	Nomenclature	MHTGR [m]	1/16th VHTR [m]
Bottom of the lower plenum	Reference	-2.88255	0
Bottom of the lower reflector	L_{RB}	-1.9825	0.05625
Bottom of the core	L_{CB}	0	0.18016
Top of the core	L_{CT}	7.93	0.6758
Top of the upper reflector	L_{RT}	9.516	0.7749
Top of the upper plenum shield	L_{T}	12.6656	0.9718
Height of upper plenum		3.1496	0.197
Reactor vessel inner diameter	D_{RV}	6.534	0.4083
Core barrel inner diameter	D_{CID}	5.95	0.370
Coolant channel diameter	D_{Hole}	0.01588	0.01905
Number of coolant channels	$N_{Coolant}$	11000	25
Coolant channel flow area [m^2]	$A_{Coolant}$	2.177	0.00713
Coolant Channel pitch	P	0.0322	0.03861
Pitch to diameter ratio	P/D_{Hole}	2.03	2.03

II.2. Particle Image Velocimetry (PIV)

Particle Image Velocimetry (PIV) is one method by which flow in a particular part of a system can be measured. It is a non-intrusive technique that seeds particles into the system and can measure both small and large fields. After particles are injected into the system, high power light beams produced from a laser and a high speed camera records movement of the particles. Images are taken from the camera are analyzed to resolve the velocity field of the system [15]. Figure 6 outlines the procedure.

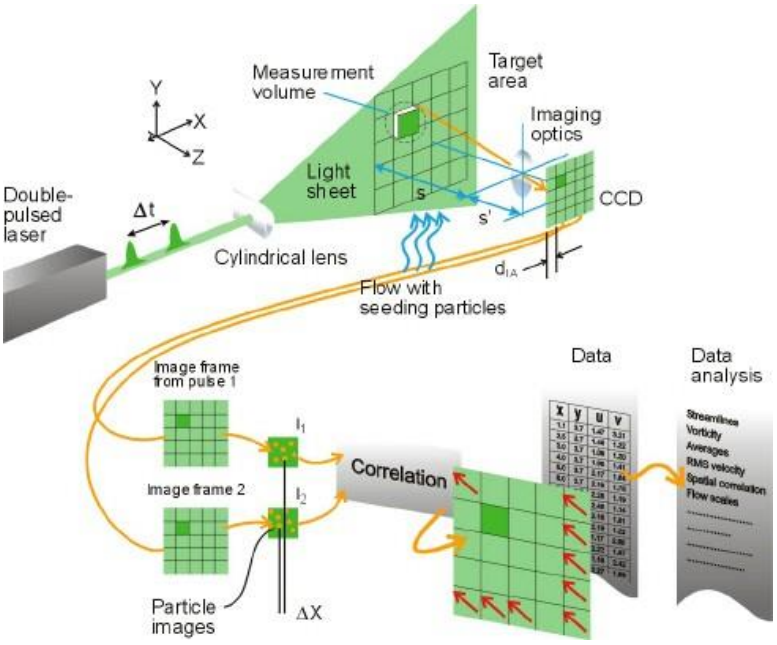

Figure 6. Scheme of PIV.

Particles used must be small enough to follow the flow without preventing it, and at the same time must be large enough to be seen by the camera. The size and type of particles depends upon many factors such as the speed of the flow and the geometry of the system. In addition, particles should be reflecting spherical particles that are homogenously distributed with uniform displacement. The density of particles should be correlated to the flow [15].

PIV can measure both liquid and gas flows, depending on the seeding material used. For liquid flow, liquid particles are mixed with water and injected directly to the flow. Table 3 gives an overview of the seeding materials used for liquid flow [16].

Table 3. Seeding materials for liquid flow.

Type	Material	Mean diameter in um
Solid	Polystyrene	10-100
	Aluminum flakes	2-7
	Hollow glass spheres	10-100
	Granules for synthetic coating	10-500
Liquid	Different oils	50-500
Gaseous	Oxygen bubbles	50-1000

PIV calculates velocity based on:

$$u(x,t) = \frac{\Delta x(x,t)}{\Delta t} \tag{II.6}$$

Where, Δx is the displacement of a particle located at *x* at time *t*, over a time Δt [17].

Figure 6 shows the scheme of the principle PIV technique see Figure 7 [18].

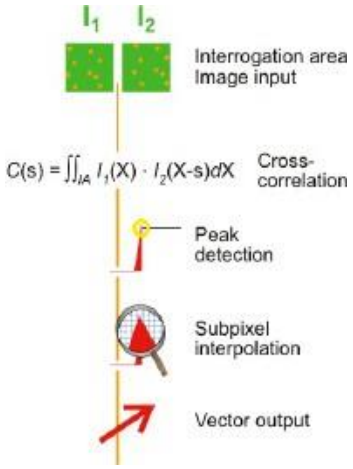

Figure 7. PIV principle technique.

For analysis, images taken of particles are divided into very small areas called interrogation areas and each area is cross-correlated. The cross correlation equation is:

$$C(s) = \iint I_1(X) \cdot I_2(X - s)dX \tag{II.7}$$

This equation generates a peak and based on this, a velocity vector is produced. By doing this many times, a map of vectors for all of the system is derived that illustrates flow characteristics.

The light source for PIV may be either a continuous laser or a pulsed laser. The continuous laser (or wave) works with normal power and no synchronization required. Pulsed laser requires a high power and a low frequency of repetition [16]. The camera used for imaging clearly must have the ability to record the small particles; in general, any high speed camera will do the job. Once images of particle flow are collected, they must be analyzed using software; many free and commercial software programs exist to do this.

II.3. Particle Tracking Velocimetry (PTV)

A second technique used to study flow is Particle Tracking Velocimetry (PTV) is. PTV uses similar components to PIV (specialized seeding particles, laser light source, high speed camera, imaging software), but calculates flow based on Lagrangian measurement this procedure is illustrated in Figure 8. This means that each particle can be tracked with time. Velocity is thus calculated as [19]:

$$\vec{v}(x(t), t) = \frac{d\vec{x}}{dt} \tag{II.9}$$

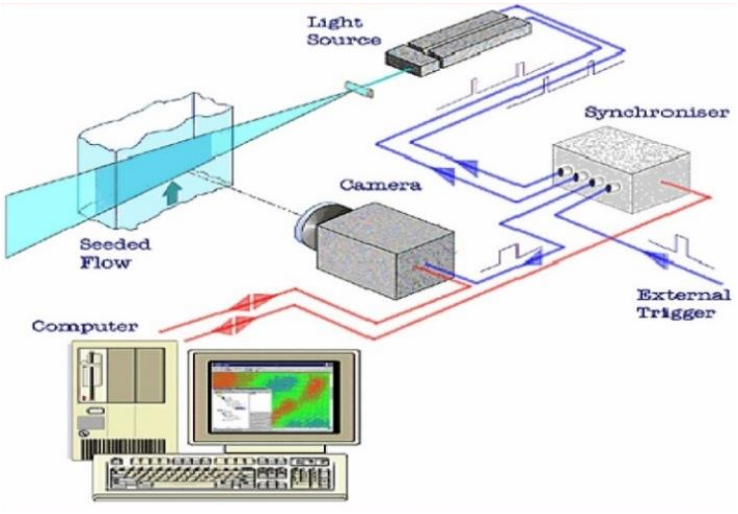

Figure 8. Scheme of PTV.

PTV seems to give an accurate result when particle density is low, giving it the ability to track particles separately. In some software, choosing the low image density mode of PIV actually means using PTV methods. On the other hand, PIV has the ability to work with high particle density, since PIV calculation depends only on the overall displacement between two images [20].

CHAPTER III

TEST FACILITY AND EXPERIMENT SET UP

III.1. Test Facility

Texas A&M test facility was designed to study the flow at the upper plenum of a VHTR by scaled to $1/16^{th}$ of its original size. Data from INL were used to help guide the scaling process. The test facility is designed to create a closed loop system, driven by natural convention under DCC accident. The main parts of the test facility are illustrated in Figure 9.

1. Upper Plenum.
2. Core with 25 pipes.
3. Cooling Jacket.
4. Water reservoir.
5. Autotransformers panel.

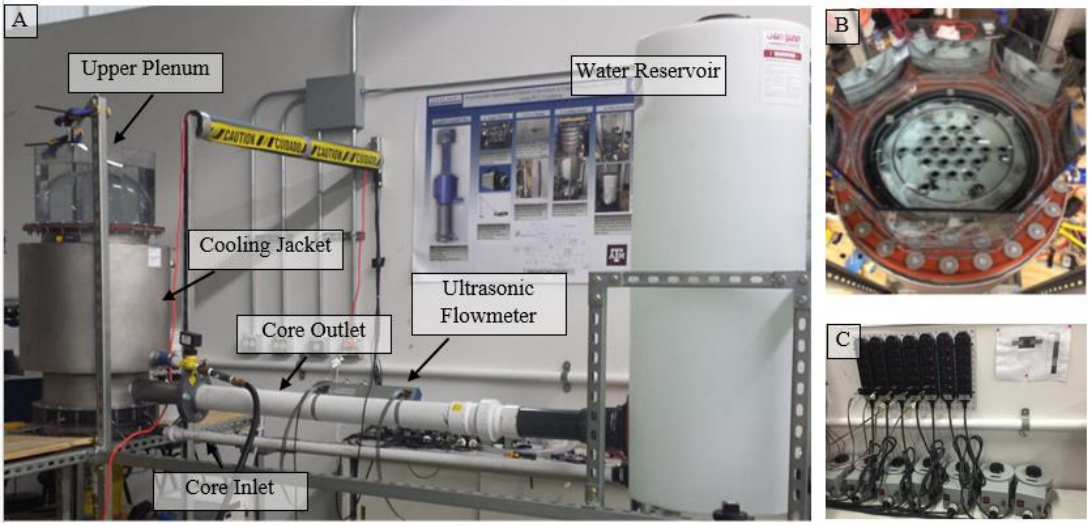

Figure 9. A: Overview of the experimental setup. B: Core with 25 pipes. C: Autotransformer panel.

Room temperature water is transported from the water reservoir to the core inlet. The water then enters into the core vessel, where there are 25 pipes (each pipe has inner diameter [ID] of 1.9 cm, and is 71.7 cm long). At the inlet pipe, a thermocouple type T measures the temperature. The pipes are then heated by heat tapes that are connected to the variable autotransformer to control the heat. Then, the water either goes to the upper plenum or lower plenum (in this case lower plenum means water goes to the core outlet). The effect of the heat generates natural convection. Natural convection, sometime referred to as buoyant convention, moves the fluid because as water changes in temperature, it changes density, causing it to become more buoyant leading water to flow into the upper plenum, which is the region of interest. At the core outlet pipe, another thermocouple type T measures the temperature. Subsequently, the flow exits the core. An ultrasound flow meter was used to record the flow at the core outlet. The

cooling jacket around the core removes most of the heat input, allowing the system to reach a steady state.

III.1.1. Upper plenum

The upper plenum was originally designed as a hemisphere since the VHTR upper plenum is a hemisphere. However, due to fabrication limitations, the upper plenum was had to be redesigned to be a cylindrical piece that was then connected to a hemisphere. The glue between the connections provides unrealistic particle data, so in PTV pre-processing, a mask was used to cut-off data collection from this area. Also, for the camera to easily capture particles in its image, a correction box, an octagon formed of glass plates, was designed to surround the upper plenum. See Figure 10.

Figure 10. Upper plenum with the correction box.

III.1.2. The core

The core is where all the 25 pipes (the fuel) is installed and the head is generated in. It is connected to the upper plenum for up and in the lower part is connected to the core inlet and output. It has at the middle bottom of at an exit where all the water is drained after the test is completed. In addition, the bottom has 25 holes each hole is .075" so the 25 pipes can be installed in it. As the fuel assembly in the VHTR core is a hexagonal shape with 1020 fuel blocks, the scaled VHTR has 25 block at the hexagonal shape. The 25 pipes are arranged into 5 groups of 5 blocks each, according to location: top (T), bottom (B), right (R), left (L) and center (C) (Figure 13). For the pipes, each pipe has two small holes, an output hole near the top and an input hole near the bottom, where thermocouples are installed. Each thermocouple was labeled according to its position, using 'b' (bottom) for the input label and 't' (top) for the output label (t) was given. For example, for the pipe at the very center, which is in group C number 1, the output label is C1t. Figures 11-13 show details of the core and the pipes. See Figure 11Figure 12 and 13.

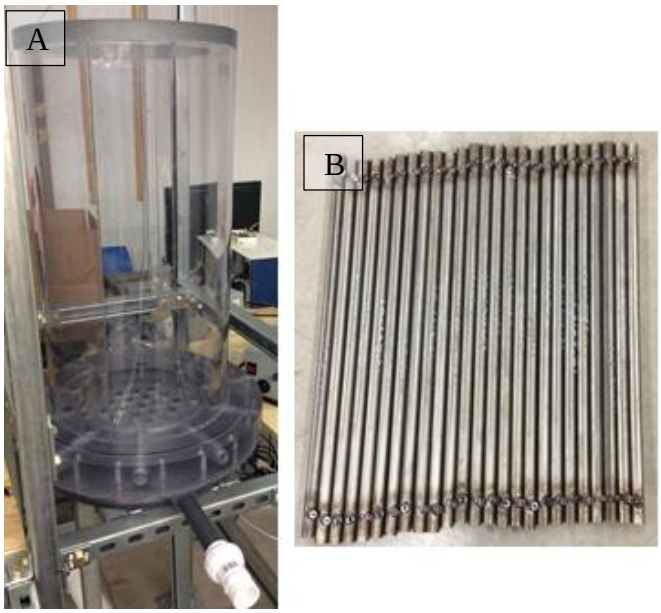

Figure 11. A: The core B: The 25 pipes.

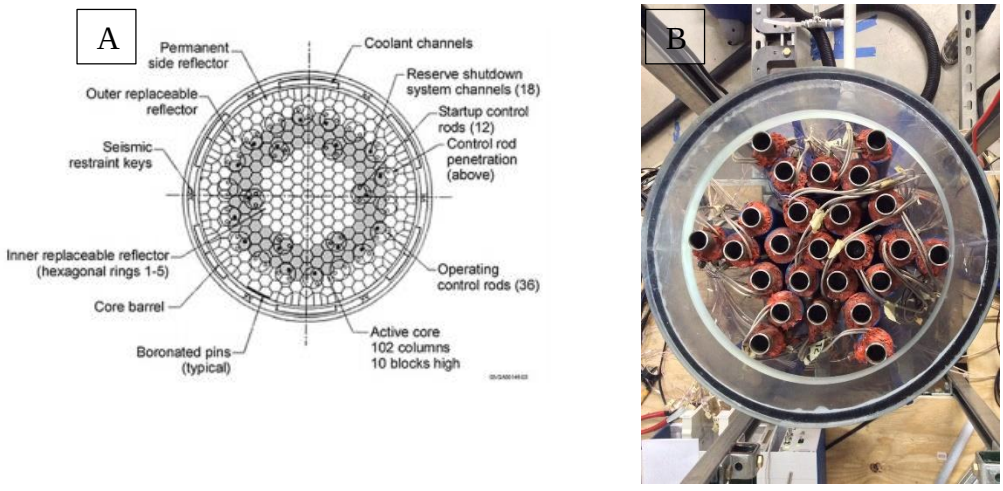

Figure 12. A: The core of VHTR B: The experiment core.

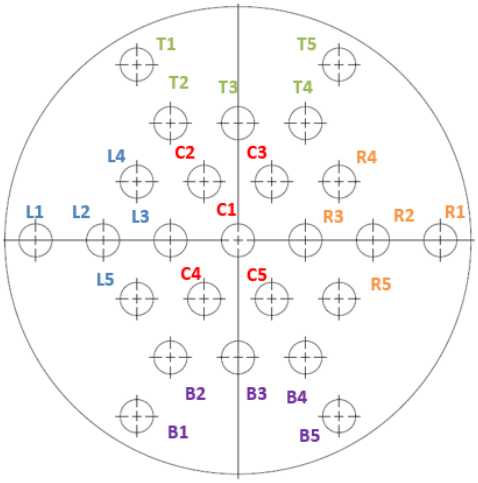

Figure 13. The core grouping.

III.1.3. The cooling jacket

The cooling jacket is made of stainless steel (a high thermal conductivity material) and installed around the core to cool the core and remove heat from the fluid. Water enters the cooling jacket from the input, moves around the core and then exits at the output. Water is pumped from the input at the bottom and then, through a series of baffles, moves to up to the output. Figure 14 is the cross section of the core with the cooling jacket.

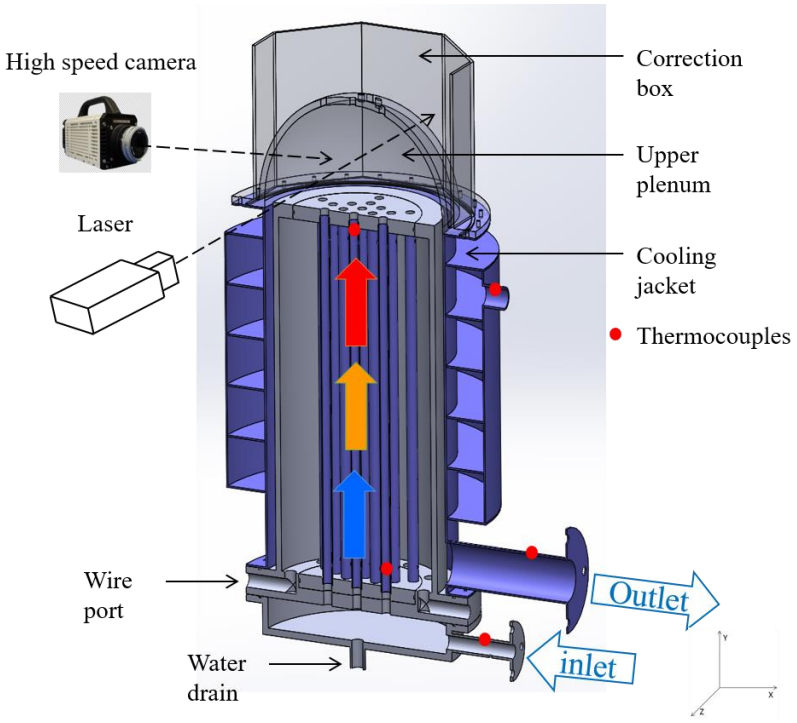

Figure 14. The cross section of the core, upper plenum and cooling jacket.

III.1.4. The water reservoir

The water reservoir is a plastic 45 gallon-tank approximately 20” in diameter. Water from the reservoir flows to the core through the input pipe and is returned to the reservoir through an input located at the up of the tank.

III.1.5. The autotransformer panel

The autotransformer panel as shown in Figure 15 holds all variable autotransformers and their connection to heat tape wires. Those will be covered in detail in the next section.

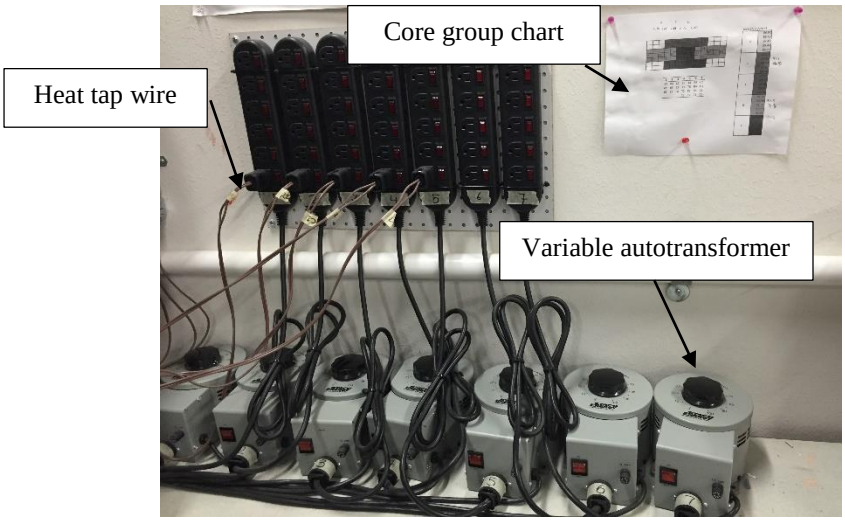

Figure 15. The autotransformer panel.

III.2. Instrumentations

This section covers the main instrumentations used to run the experiment. which are:

1. Thermocouples.
2. Flowmeters.
3. Heat tapes.
4. Variable autotransformer.
5. Differential pressure transducer.
6. Data Acquisition System (DAQ).
7. Laser.
8. High speed camera.

III.2.1. Thermocouples

A thermocouple is a wire that measure temperature. It contains two wires made of different materials, and measures temperature by generating a voltage associated with temperature. A mathematical equation is then used to convert the voltage reading to temperature. Figure 16 is the thermocouple was used in the test.

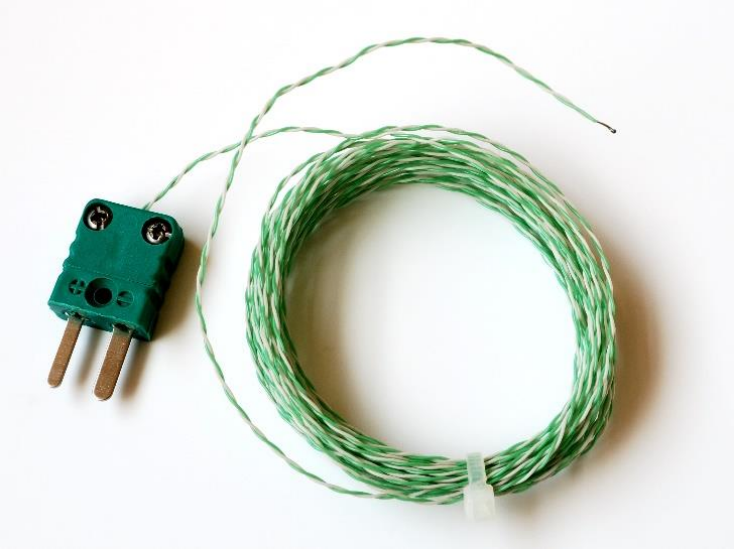

Figure 16. Thermocouple wire.

There are several types of thermocouples that vary in features such as temperature range, resistance to vibration, and others features that depend on the application. Type K, J, T, E thermocouples are the most commonly used [21]. In this experiment, 54 thermocouples type T from OMEGA were used. Its wire is made of copper and a constant. It has an uncertainly of ± 0.5 °C, and its temperature range is

from -210 to 760 °C. Fifty thermocouples were used for the pipes – one for each inlet and outlet in each. Another four thermocouples were installed in the inlet of the coolant jacket, the outlet of the coolant jacket, the core inlet and the core outlet. All thermocouples were labeled with unique identifiers.

Two wires in the thermocouples should be joint together by using a wire welder for thermocouples to work, the two wires inside must be joined together using a wire welder. To insure that there were no leaks into the thermocouples, which were in contact with the water, the end of the thermocouples were sealed inside a compression fitting. This was done by cutting a fine steel tube and inserting it into the thermocouple. A UV epoxy, a liquid chemical material that turns solid after being exposed to heat, was applied, heated by a UV light (Ultraiolet), and then ferrules were installed on the tube (Figure 17).

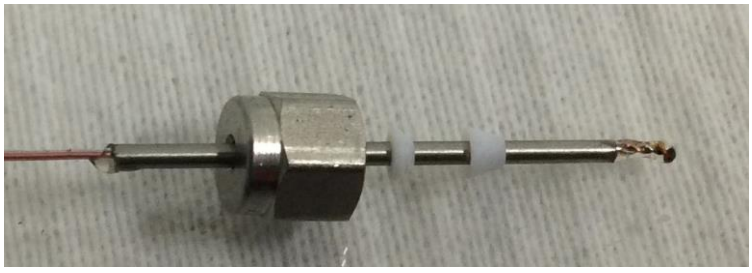

Figure 17. View of a prepared thermocouple.

Thermocouples need to be calibrated. To do so, thermocouples were inserted into a water at three temperatures: room, cold and hot. All temperatures were monitored by

FLUKE 52 II thermometer. FLUKE as shown in Figure 18 is a thermometer that has a thermocouple as a sensor and has the ability to give a quick dual temperature measurement at an accuracy of ± 0.3 °C. In addition, to calibrating the thermocouples, the FLUKE thermometer was used to measure the temperature at the correction box and in the water reservoir.

Figure 18. FLUKE II 52.

III.2.2. Flow meters

A flow meter is a device measure that measures flow rate inside a pipe. Two types of flow meters are used in this experiment.

III.2.2.1. Ultrasound flow meter

The ultrasound flow meter (manufactured by Krohne) uses an ultrasound transducer to measure flow inside a pipe. This type of flow meter was used for its non-intrusive method to measure flow at the core inlet.

As the flow in our system is less than the company tested range, the company recommended that we calibrate the device in the lab. To do so, a separate pipe with the same dimension as the pipe used in the experiment was bought and the ultrasound flow meter was clamped to it. The flow meter was then calibrated using the Optiflux 1000 electromagnetic flow meter. The electromagnetic flow meter has an uncertainty of ± 3%. An excel spreadsheet was used to record 10 different flow rates.

Figure 19 shows the calibration set up, and

Figure 20 gives the relationship between the electromagnetic and ultrasound flow meters.

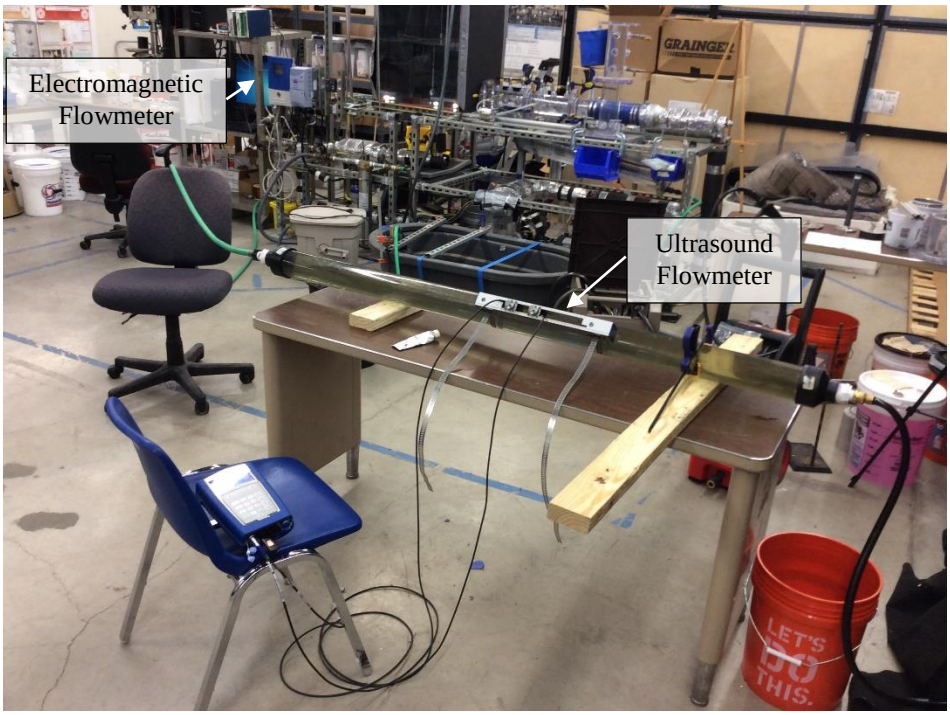

Figure 19. Ultrasound flowmeter calibration.

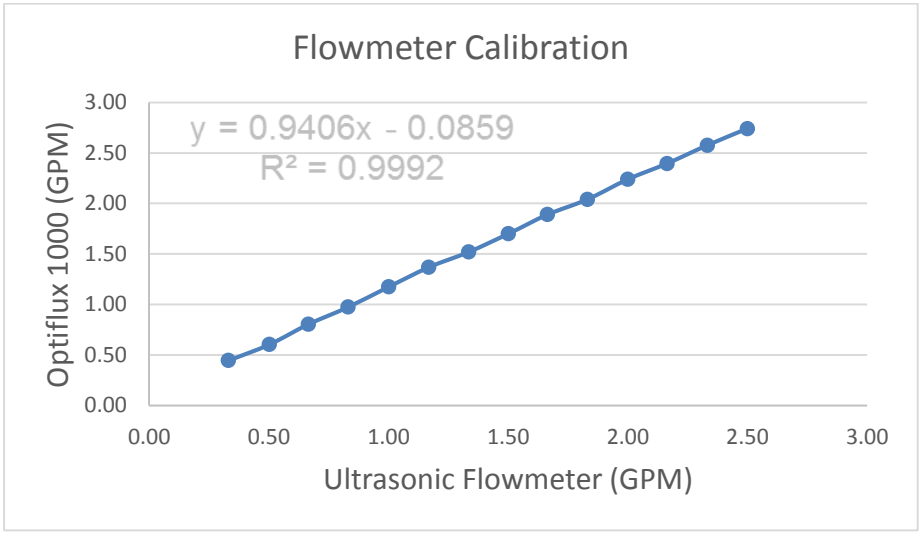

Figure 20. Calibration plot for the ultrasound flowmeter.

III.2.2.2. Paddlewheel flow meter

The second type of flow meter used in this experiment was a paddlewheel flow meter, is a device that is installed within the system to measure flow rate. It works with a small impeller, and the flow inside the pipe push the impeller to generate a frequency and voltage that is then it converted to relative flow rate. High voltage means high flow rate. Figure 21 shows the paddlewheel principle work.

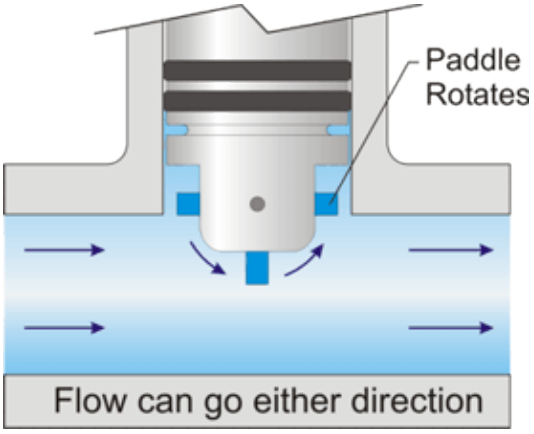

Figure 21. Paddlewheel principle.

A Blue White F-1000-RB was used to measure flow at the cooling jacket inlet. Since the the cooling jacket inlet is open at the inlet to connect the hose to cool the system, a paddlewheel flow meter could be installed without affecting the system, as shown in

Figure 22. The flow meter has an LCD output with 6 digits (up to 4 decimal places) and operates with two batteries. The flow meter had an update time of 1.5 sec, comes already calibrated and with different pipe sizes. For the technical standards, see Table 4.

Table 4. Blue White F-1000-RB technical standards.

Flow ranges	0.4 to 200 GPM
Maximum working pressure	300 psig
Maximum fluid temperature	93°C
Maximum pressure drop	8 psi
Uncertainty	± 2%

Figure 22. Blue White paddlewheel contacted to the cooling jacket inlet.

III.2.3. Heat tapes

In VHTR, the core is heated when the fuel interacts with neutrons. In this experiment, pipes were heated to simulate the heat in VHTR using heat tapes. Heat tapes, or electric trace heating, generates heat to the tape by applying voltage. Each pipe was surrounded with tape and connected to the power supply. To keep it safe and to reduce heat loss, each heat tape wrapped pipe was surrounded with a high temperature silicon tube, and sealed with high temperature adhesive as seen in Figure 23.

Figure 23. A. Heat tapes around the pipes, B. High temperature silicon tubes to seal the pipes.

III.2.4. Variable autotransformers

Heat tapes require a power source to generate heat and in this experiment, heat needs to vary depending on the total power required. This was done using variable autotransformers. Figure 24 shows the variable autotransformers was used.

Figure 24. Variable autotransformer.

In this experiment, a total of 10 kW of power are needed in the system. Thus, dividing the total power (10 kW) by the number of pipes (25) gives 0.4 kW for each pipe. Each heat tape has its own resistance; by grouping tapes of each similar resistance into one group, seven groups, each with its own average resistance, are formed and each group has it is own variable autotransformer. However, in this experiment only one heat tape has been used, so the exact resistance has been taken into account.

To find the current needed to have 0.4 kW per pipe, the equation

$$I = \sqrt{P/R} \quad \text{(III.1)}$$

is used, where I is the current in amperes, P is the power in watts, and R is the resistance in ohms. By using a Yokogawa CL120 clamp on an AC current tester, the current required is achieved by rotating the variable autotransformers.

III.2.5. Differential pressure transducer

The differential pressure transducer is a device to measure pressure at two different places. In this experiment, it is installed at the inlet and outlet of the core as shown in Figure 25. I used Honeywell model KZ, which has 0.25% accuracy and can measure from 0.5 to 30 psid.

Figure 25. Honeywell differential pressure transducer.

Power was supplied to the pressure transducer with a Tenma TS3510P single channel power supply with 10 Volts and 1 Ampere, as shown in Figure 26.

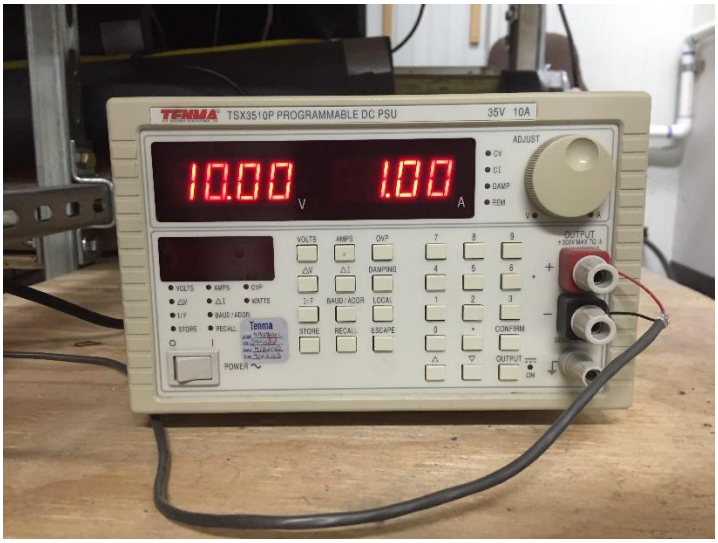

Figure 26. Tenma single channel power supply.

III.2.6. Data Acquisition System (DAQ)

All thermocouples and the differential pressure transducer output needs to be connected to a device that can collect all the data and convert it to a system for analysis. This device should have the ability to minimize reading error while reading and recording measurements at frequent intervals. A Data Acquisition System (DAQ) can do all of this and in this experiment, DSA from National Instruments NI SCXI-1001 was used see Figure 27. This device could be used for both thermocouple calibration and reading of the data.

The NI SCXI-1001 has a 12 slot chassis. It uses AC power and has two cooling fans. National Instruments claims this DAQ is ideal for high channel counts. The chassis is the most important part in the system, as it is the connecting link between the

thermocouples and the software. It works by converting all data from the thermocouples from voltage into temperature before sending it to the software. The chassis was also connected to a control module that is in turn connected to the thermocouples output. A type SCXI-1303 was used as a control module. It is designed for high accuracy thermocouples measurements using isothermal. Each module can take up to 32 thermocouples. In this experiment, three control modules were used. All data was saved to a text file using NI's LabVIEW software; data were recorded every second.

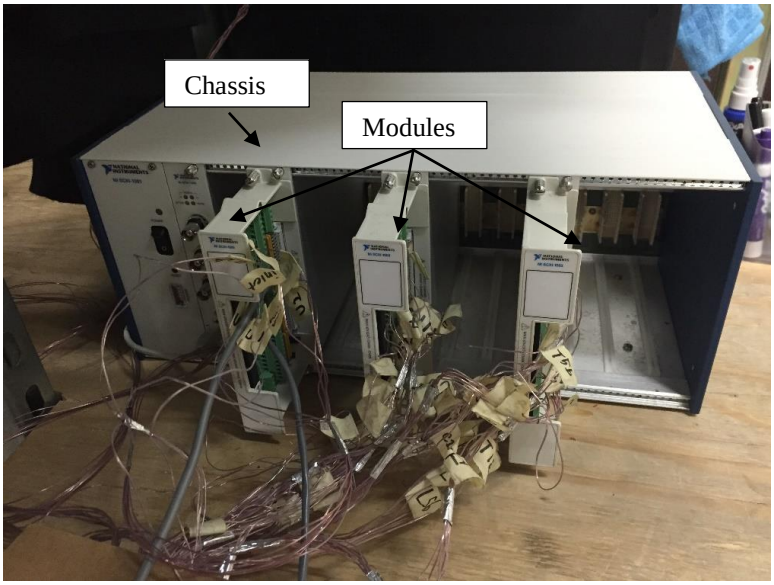

Figure 27. NI DAQ.

III.2.7. Light source (laser)

The light source is a crucial component in the PTV system. In this experiment, a new wave research Solo III-15 dual-laser was used. It contains both a cooling system

and the laser system. Its output energy is 50 mJ with ± 4% stability of the power, its frequency is 10 Hz, and beam diameter is 3.5 mm. For the required operation, the temperature needed to be approximately 21 ± 0.5 °C and required voltage range was range from 95-240 V with 50/60 Hz. Figure 28 illustrates the laser system.

Figure 28. Solo III-15 laser system.

III.2.8. High speed camera

The second component of the PTV system is the high speed camera. When particles is injected and the laser is on, a camera is used to record the particle positions in the system. The high speed camera MEMRECAM GX-3 from NAC image technology as shown in Figure 29 was used for this purpose. Its maximum image size is 1280 x 1024 pixels. The camera should be calibrated to convert the pixel into cm. To calibrate the camera for converting pixels into cm a stick with two marks was placed into the upper plenum and picture taken of it. By using camera software and knowing the length of the two marks, the pixel to cm conversion is easily calculated.

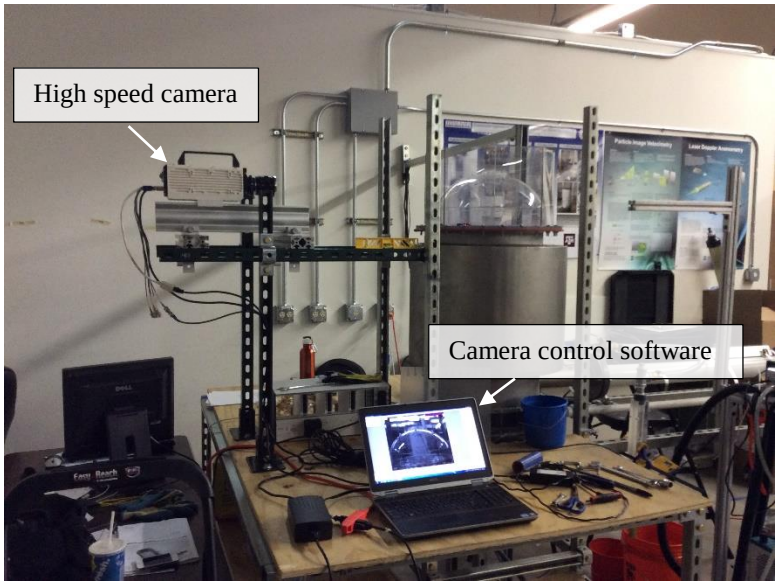

Figure 29. High speed camera MEMRECAM GX-3.

III.3. Safety

Safety is an important concept in any project. In this experiment, many safety elements are added to the system to insure the safety of the worker and the instruments.

First, the system is never operated alone. At least two people should be in the lab. This reduces the possibility of mistakes that can lead to a dangerous situation. In addition, the experiment is not run without anyone around it. To do so, the offices of the workers were moved near the station.

Second, all the wires are connected in a safe way. This experiment needs a lot of wires plugged from the experiment to either an autotransformer panel or an electrical outlet. To do so safely, all wires were protected by building them a route that was far from the ground.

Figure 30 illustrates this.

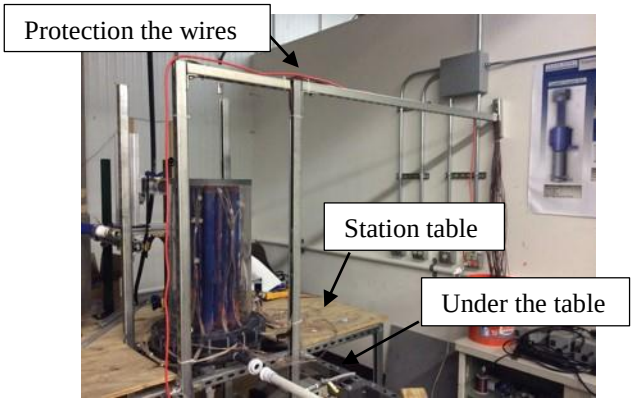

Figure 30. Safety of the wires and instruments.

Third, to protect all the instruments from water that might spill over from the upper plenum, all the instruments were either located not too close to the core or under the station table (see

Figure 30).

Finally, a laser was used in this experiment and many safety guides are required to operate a laser. A training course about general laser safety offered by Texas A&M University was required for all who work in this experiment. All workers are required to wear laser safety goggles to operate the laser. In addition, a black curtain surrounds the experiment area when the laser is on. These precautions reduce the possibility of accidental damage to human eyes from the laser see Figure 31.

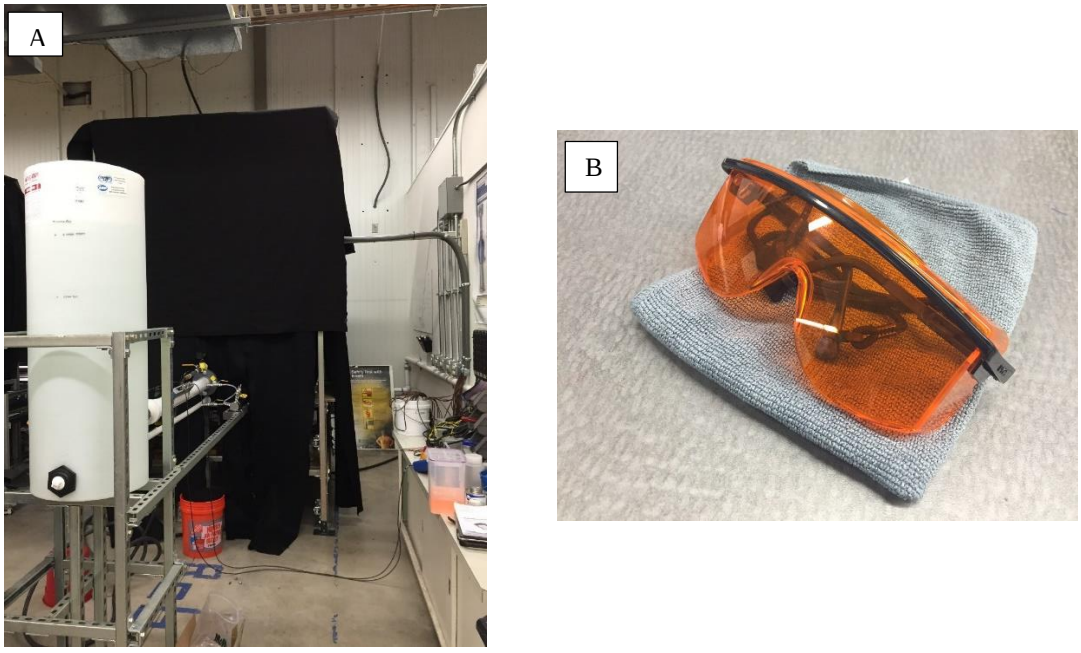

Figure 31. A. Black curtain, B. Laser goggles.

III.4. Particles

Particles are key to the PTV system. Also, particles should be bright when the laser beam is on them. In this experiment, 53–63 μm fluorescent orange particles in polyethylene microspheres with a density of 1.002 g/cm^3 were used. Particles are re-used by using, two sieves (0.990 mm and 0.045 mm) at the drain tank to filter water as it drained, collecting most of the particles. Figure 32 shows both the particles' container and the microsieves used.

Figure 32. A. Particles container, B. the micro-sieves used to collect particles at the end of the test.

CHAPTER IV

TEST AND RESULT

IV.1. Test Procedure

The goal of this is to study the phenomena of one jet in the reactor core. Thus, only the center pipe (C1) was studied and all the other pipes were closed.

To start the test, first full the water in the water reservoir. Wait until the water goes to the core and fill the upper plenum. Take a look into all the system to make sure there are no leaks. Any leaks found must be repaired before continuing. If no leaks are present, record the temperature at both the upper plenum and reservoir by using Fluke thermometer and record the temperatures in an excel sheet. At the excel sheet the date and the time of start the water and measure the temperature were documented. Add a little bit of particles. Mix particles with water and use a syringe to inject them into the core. Mount the laser, insuring it is in line the center pipe and mount the camera to face the laser sheet. Next, test the camera image by zooming the camera to the upper plenum and the pipe being used. After making sure the PTV system is ready to work and installed correctly, turn on the heat. This is done, by increasing the voltage of the heat tape gradually to achieve the desired power level, 0.4 kW, by measuring the input current of the heat tape. Simultaneously, start recording in the ultrasound flow meter. The ultrasound flowmeter is synchronized with the computer time.

The temperature for the core was monitored using the LabVIEW program for DAQ. The steady state was defined as the point at which difference in temperature

between the inlet and outlet was 0 ± 0.5 °C. At this time, the cooling jacket was turned on remove the heat. To reduce the heat loss in the core such that it is negligible, hot water was added to the correction box. At the upper plenum with the heated flow, small bubbles may be generated. Reducing or removing these bubbles gave more accurate pictures. This was done by using a small stick inserted into the upper plenum that was rotated to stir water.

Turn on the laser and the camera took the pictures for 5 minutes. At the excel sheet, the time the camera recorded and finished were written.

After testing, to shutdown the system, the laser and camera system are first turned off. Then, the autotransformers, the ultrasound flow meter and DAQ system are all turned off. Finally, the water is drained; at least one person should remain at the test area until all the water is drained.

IV.2. Analyzing

Code written in-house using visual basic (Microsoft®) was used to process PTV data. The code includes an algorithm with three main parts. The first concerns particle detection. Particles were detected based on intensity, using a particle mask correlation method.

$$I(x,y) = I_0 \exp\left[-\frac{1}{2r_0^2}\left(\frac{(x-x_0)^2}{a^2}\right) + \left(\frac{(x-x_0)(y-y_0)}{c^2}\right) + \left(\frac{(y-y_0)^2}{b^2}\right)\right] \quad \text{(IV.1)}$$

Where, *I(x,y)* is the intensity at the *(x,y)* position,

(x_0,y_0) is the centroid location of the particle,

I_0 is the maximum intensity,

a, b, and c are shape modifier parameters.,

and, r_0 is the particle radius.

Once a particle was detected, particle centroid estimation (the second part of the algorithm) is used. Finally, particle tracking is the third part of the algorithm. Direct spatial correlation was used, taking two images and measuring the movement of each particle that was detected.

$$C_{IAIB}(x_0, y_0) = \sum_{i=1}^{a}\sum_{j=1}^{b}[I_A(i,j) - \bar{I}_A][I_B(i,j) - \bar{I}_B] \times \left(\sum_{i=1}^{a}\sum_{j=1}^{b} I_A(i,j) - \bar{I}_A\right)^{-1/2} \times \left(\sum_{i=1}^{a}\sum_{j=1}^{b} I_B(i,j) - \bar{I}_B\right)^{-1/2} \quad \text{(IV.2)}$$

Where, A and B are the two images,

a and b are the dimensions, and

$\bar{I}_A$ and $\bar{I}_B$ are the average intensities. [22].

The code has other features. It is easy to operate with a little bit of experience, it has a good user interface, many options to choose from, it is flexible with the system geometry and it is fast. In addition, it has a support code to filter the output vectors from the bad ones.

During preprocessing, a small number of images were selected for a preliminary test. The preliminary test was used to ascertain the appropriate correlation window, candidate window, the size of particles, and the mask. First, a mask was applied to eliminate unwanted areas such as the glued connection between the hemisphere and cylindrical, the outer part of the hemisphere, and near the inlet where many particles with zero velocity are present, as shown in Figure 33A. For the centroid of the particles and cross correlation, different cross correlations were examined by changing the particle radius, mask radius and the mask sphere. Trial and error were used to choose the appropriate input data. Also, comparison tests using both the same and different data were done as shown in Figure 33B. The code generates the output vectors for each image pair. The PTV filter is used to validate the vectors and remove all the failed vectors; interpolated vectors are then used to replace failed ones. The filter can choose a particle area or the whole system. In this test, all areas were used with size of 1280 x 1024 pixels. The software can also interpolate the number of data points desired; in this test a 100 x 100 grid output were used. The filter averaged all image pairs into two output files; one giving y, x, z, u, v, w, area, number of vectors, u standard deviation, v standard deviation, and area standard error, and the other file giving, y, z, z, u, v, u', v', $u'v'$, and number of vectors. All output was in px units, which were converted to cm and then cm/sec calculated. Converting px to cm is required to analysis the data. Convert equation is needed to convert px to cm and then px/frame to cm/sec. This was done by taking a pictures with the same high speed camera of a long stick that was installed

inside the upper plenum. Knowing the length of stick and using the camera system, a convert equation was given

Figure 34 is the image of the stick that used to convert from px to cm. To convert from px to cm output was multiplied by 0.021 and for px/frame to cm/sec, output was be multiplied by 0.207. The code is written to give the opposite the y value, so y was multiplied by (-1) to correct for this. In addition, the x axis output starts from zero. It is preferred to put the center of the jet output as a zero. This was done by subtracting from the x value with the exact location of the center pipe. Matlab was used to convert all output into cm or cm/sec and arrange the axes, as well as to combine the needed data into a single file. Finally, two output files with the same data were generated; a text data file and the Tecplot friendly file.

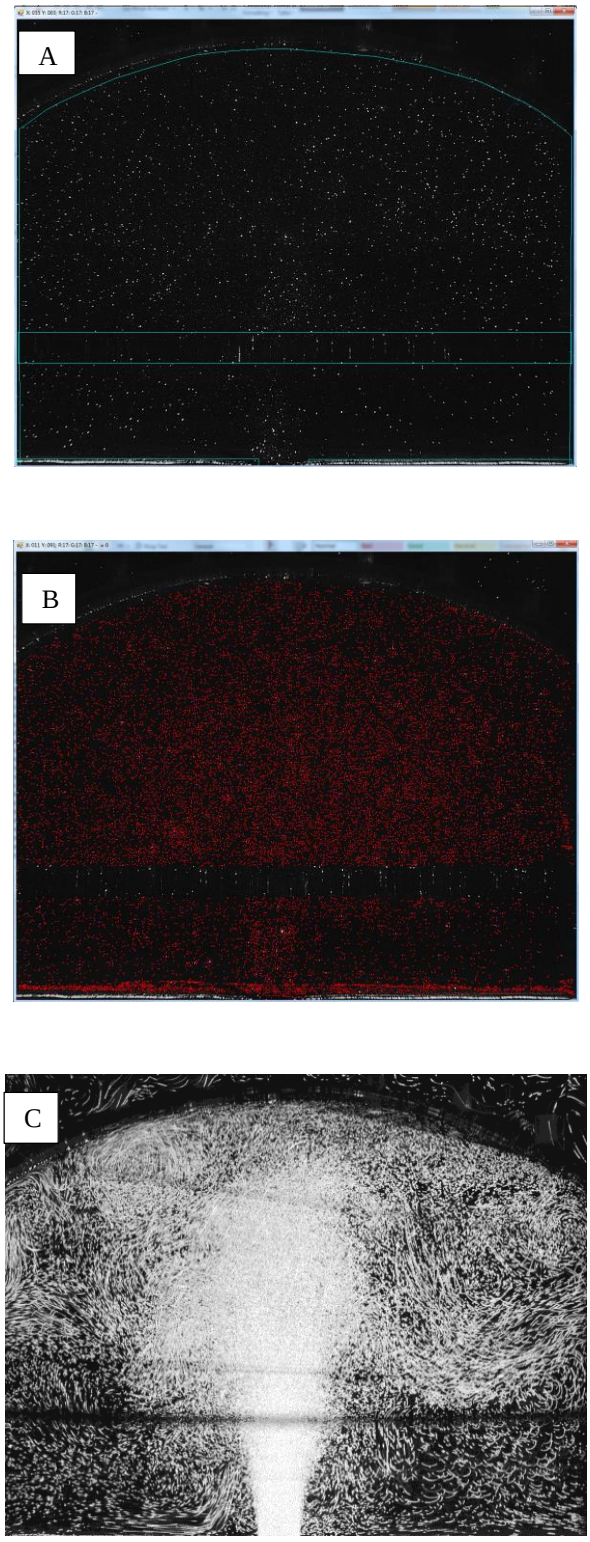

Figure 33. A. Masks with different regions B. Cross correlation window C. Particles displacements.

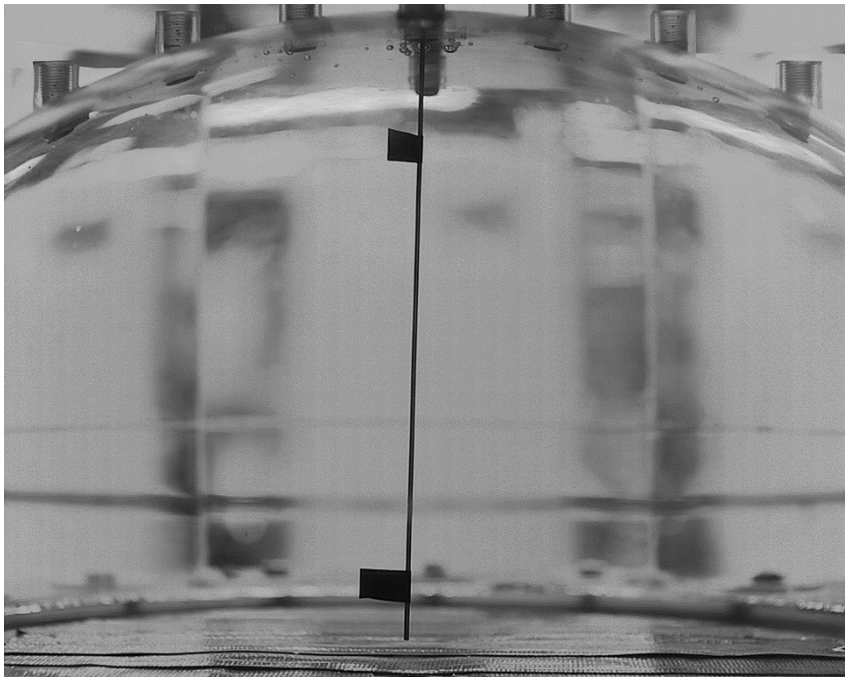

Figure 34. Calibration to convert from px to cm.

After finishing the preprocessing, a sensitivity analysis was used to estimate the number of frames required to achieve a steady state. Then, three tests were used to investigate the behavior of the flow.

IV.3. Results

IV.3.1. PTV results

After pre-processing the images, 1500 frames were used and filtered to study the flow behavior. Tecplot software was used as an animation tool to illustrate the flow movements. Figure 35 shows the velocity magnitude for one test. At 5 cm is the blocked

mask where glue is located and data were excluded. Velocity is higher in the middle of the plume, from approximately 10 to 15 cm.

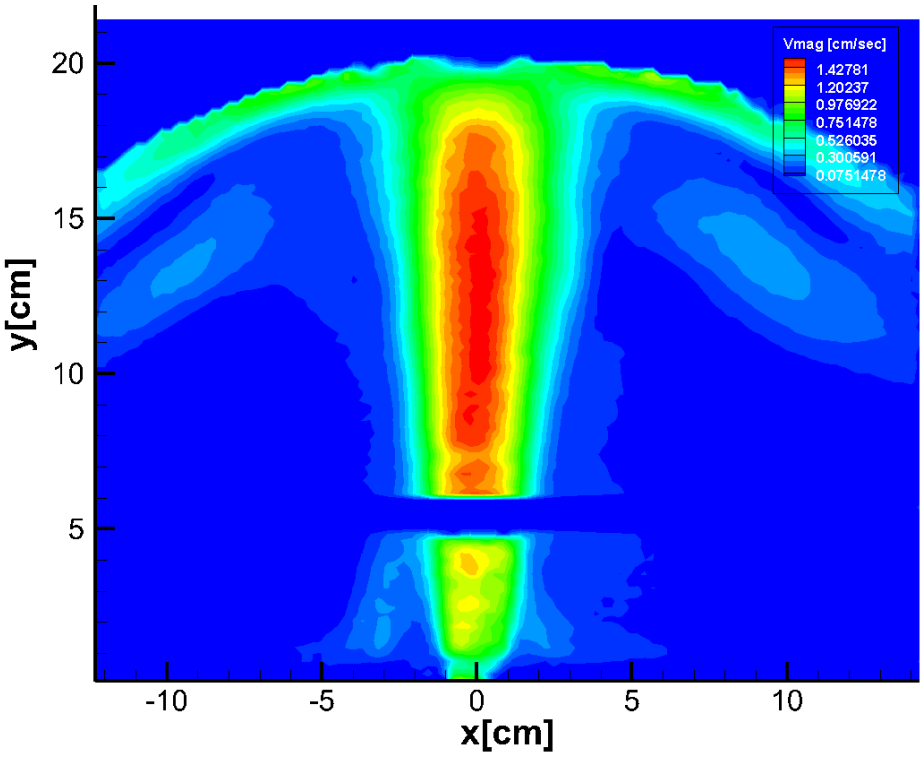

Figure 35. Velocity magnitude counter. The missing data at y = 5 cm is where the image was masked.

Figure 36 shows *v* velocity standard deviation counter for one test. Note the flow has large fluctuations near the output of the pipe. The flow is unstable especially near the glue part, ranging from 0 to approximately 8 cm, after which the flow becomes more stable. This suggests flow near the outlet has a high turbulent intensity.

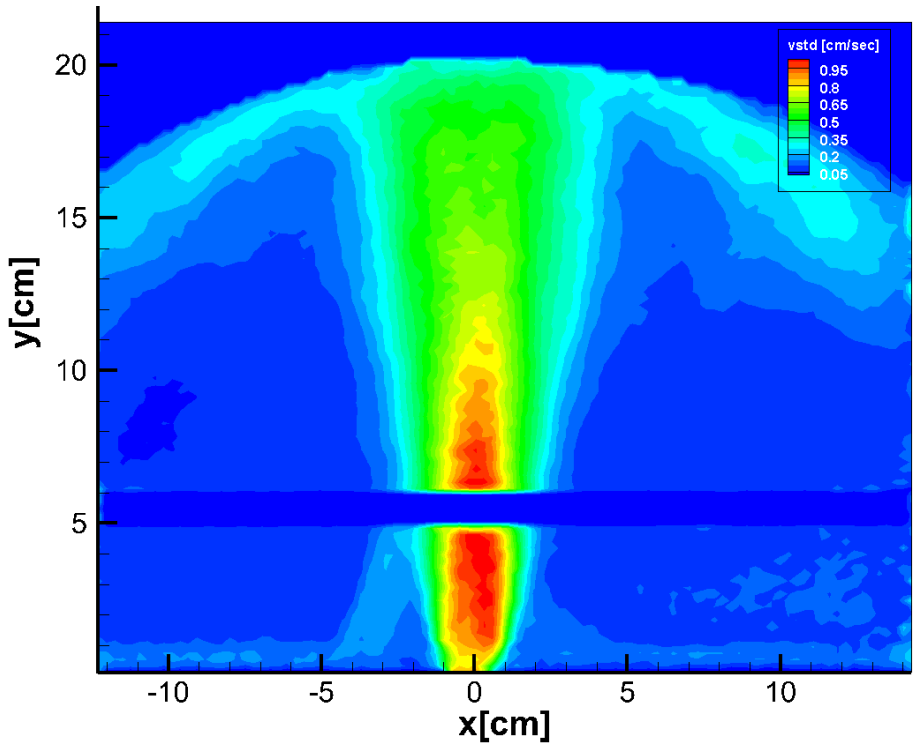

Figure 36. v velocity standard deviation counter for one test.

Figure 37 shows the streamlines for one test. For an ideal plume, one vertex should be located in each side. In this experiment, there is a second, relatively small vertex forms at the right side of the testing area. This could be because the output of the flow has a larger space on right than in the left.

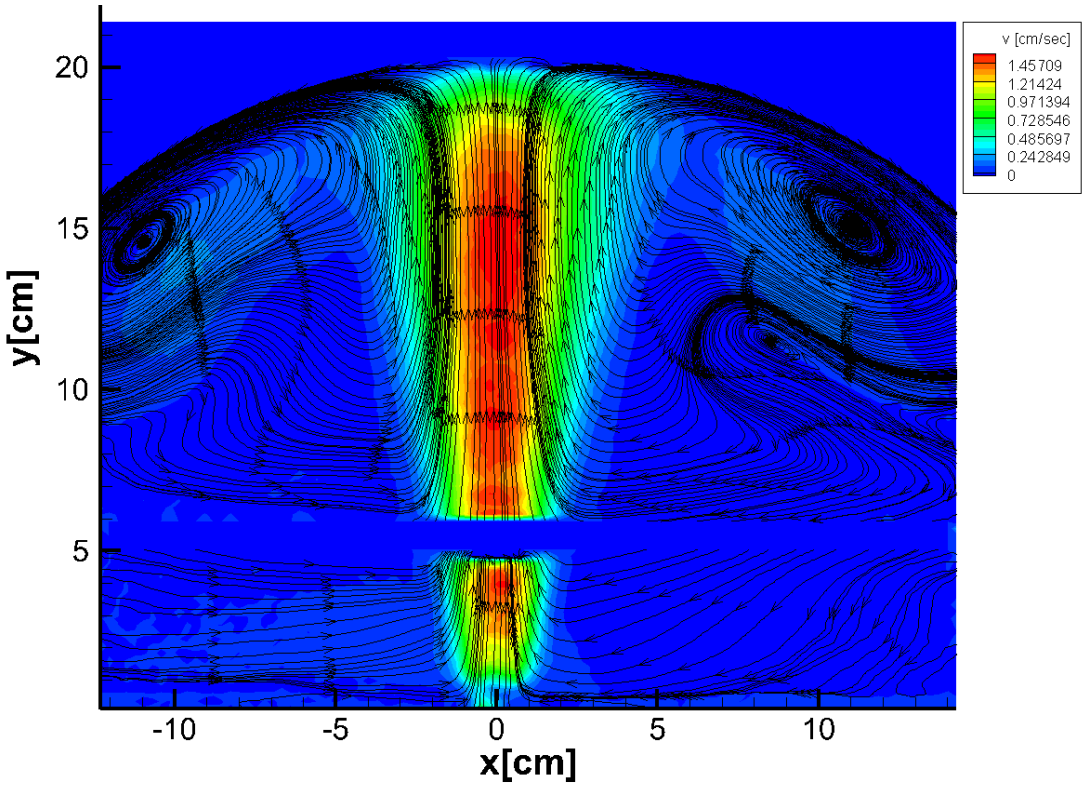

Figure 37. The streamlines for one test.

IV.3.2. Sensitivity analysis

To investigate uncertainty of each test output, a sensitivity analysis was done to ascertain the frames required to minimize error the output averages. There are multiple ways to do sensitivity analysis. An approximation error or the absolute error was calculated for output of 50, 100, 150, 250, 500, 750, 1000 and 1250 frames. In this test, 1500 frames was used as reference. This estimation is more than the well-known frames are needed to reach the steady state and give a fine average. Three tests of sensitivity

were done using data from the same experiment, but taken at different times. The equation to estimate error is:

$$Error = \frac{\sum_{i,j=1}^{n} \left| v_{i,j} - \bar{v}_{i,j} \right|}{n} \tag{IV.3}$$

Where the $v_{i,j}$ is the Y-velocity field for each frame and $\bar{v}_{i,j}$ is the 1500 frames average Y-velocity field.

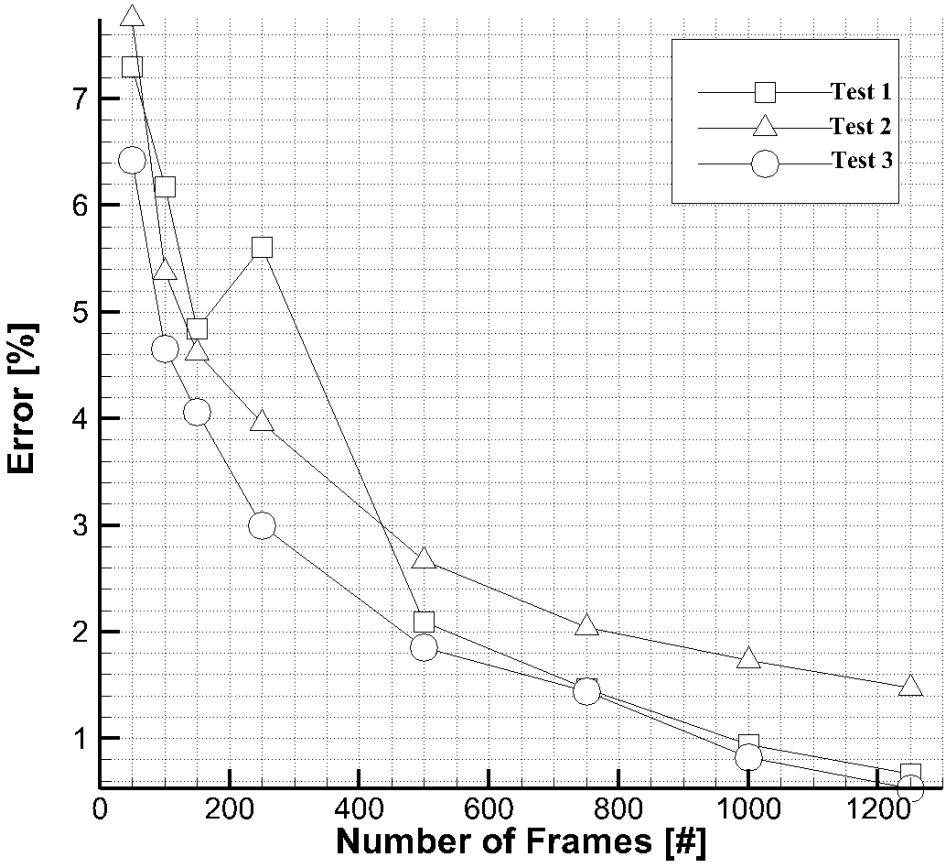

Figure 38. Percent error for the three tests of y-velocity field.

Figure 38 illustrates the error in the Y-velocity field for the three tests using different number of frames. Using only 50 frames, tests 1 and 2 had approximately 7.5% error, while test 3 had approximately 6.5%. For all three tests, error declined as number of frames increased. The sole exception to this was test 1 at 250 frames, where error increased from approximately 5% on 150 frames to 5.5% on 250 frames. This may be a phenomenon of the plume. The plume is moving right and left, so the average should be in the center. In test 1, the plume starts to move left more than right. When averaging over 250 frames, the average output shows the plume is on left rather than the right, and that is one reason why more frames are required to reach a steady state and reduce this kind of error. At 750 frames, tests 1 and 3 reach approximately 1.5% and test 2 reaches approximately 2.25%. The optimum is an error of less than 2%. As all tests have 2% or less error at 1000 and 1250 frames it can be concluded that 1000 frames are sufficient to reach a steady state and proved a precise average of the output.

Further analysis of three horizontal lines were studied for each test at y = 3, 9, and 15 cm from the pipe outlet was done (Figure 39). These locations were chosen to be far from boundaries such as the outlet and the glue part.

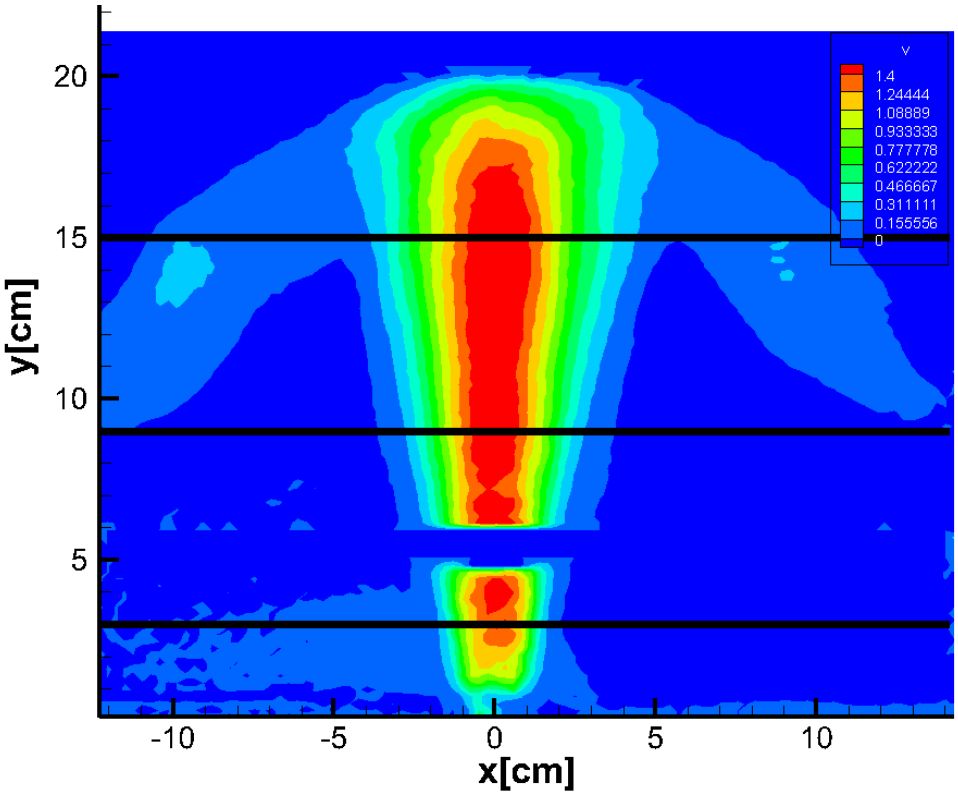

Figure 39. The locations of the line extraction

Sensitivity analysis for tests 1, 2 and 3 at y = 3, 9 and 15 cm from the pipe outlet are shown in Figures 40 to 48, below.

At 3 cm from the pipe outlet, maximum velocity is 1.2 ± 0.1 cm/sec Starting from 500 frames to 1000 frames, the velocity profile takes on the same pattern as at 1500 frames. The 50 frames and 200 frames are a little off the range of 1500 frames (Figure 40, 41 and 42).

At 9 cm from the pipe outlet, maximum velocity is 1.5 ± 0.1 cm/sec. The 50 and 200 frames estimates go outside the 1500 frames line, while the 500 and 1000 frames estimates match that of the 1500 frames (Figure 43, 44 and 45).

At 15 cm from the pipe outlet, where the maximum velocity of the plume is located, the maximum velocity is 1.6 ± 0.05 cm/sec uncertainty. The 50 frames estimate still does not accurately reflect the flow pattern. On the other hand, the remaining estimates using different numbers of frames do follow the 1500 pattern accurately (Figure 46, 47 and 48).

For the plume, the *v* standard deviation reveals that the flow has large fluctuations near the output of the pipe. This is why sensitivity analysis at 3 cm different pattern for estimates using different numbers of frames. In addition, the *v* stander deviation shows that the stability of the flow increases as it goes up; this is why most estimates at 9 cm and 15 cm were more stable across a range of frame numbers used.

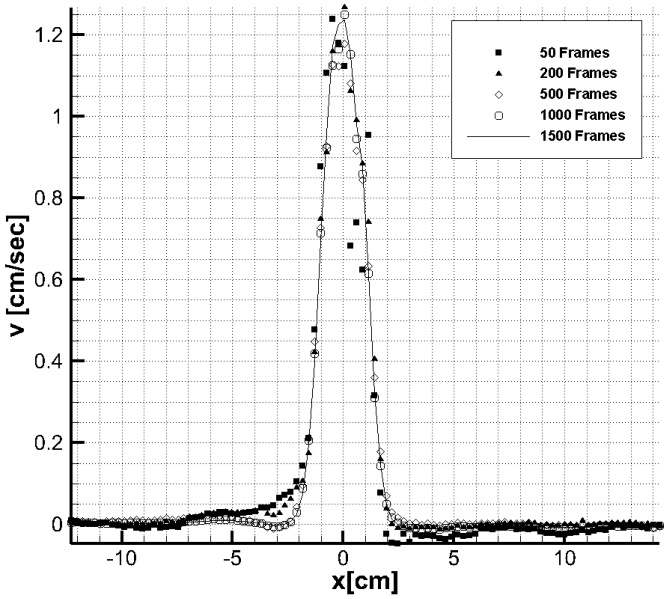

Figure 40. The sensitivity analysis at 3 cm from the pipe outlet for test 1.

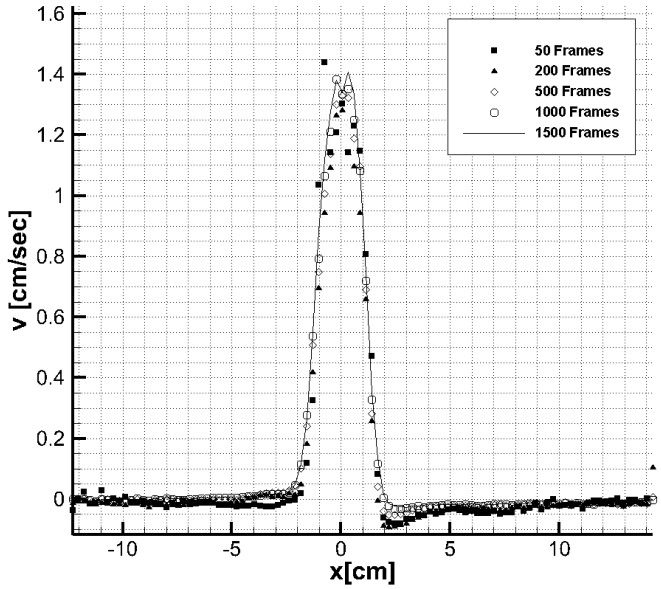

Figure 41. The sensitivity analysis at 3 cm from the pipe outlet for test 2.

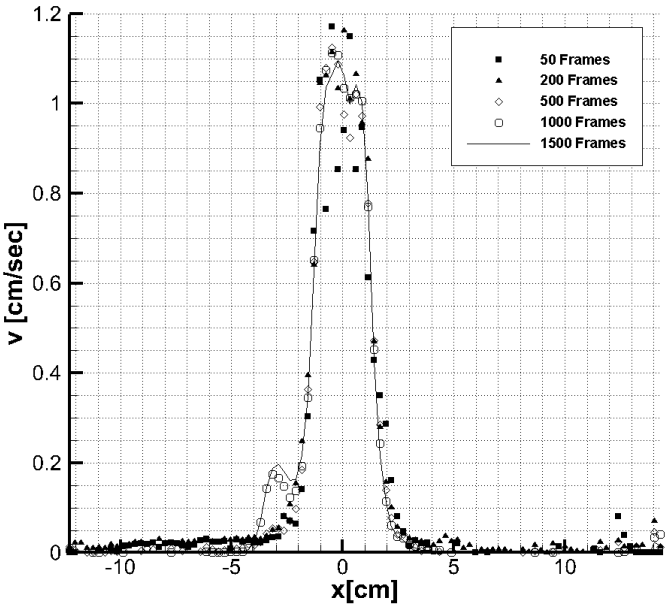

Figure 42. The sensitivity analysis at 3 cm from the pipe outlet for test 3.

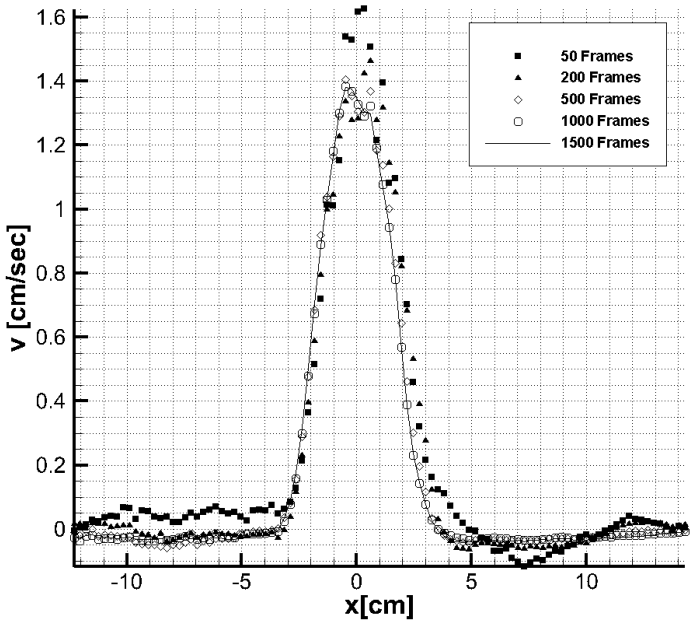

Figure 43. The sensitivity analysis at 9 cm from the pipe outlet for test 1.

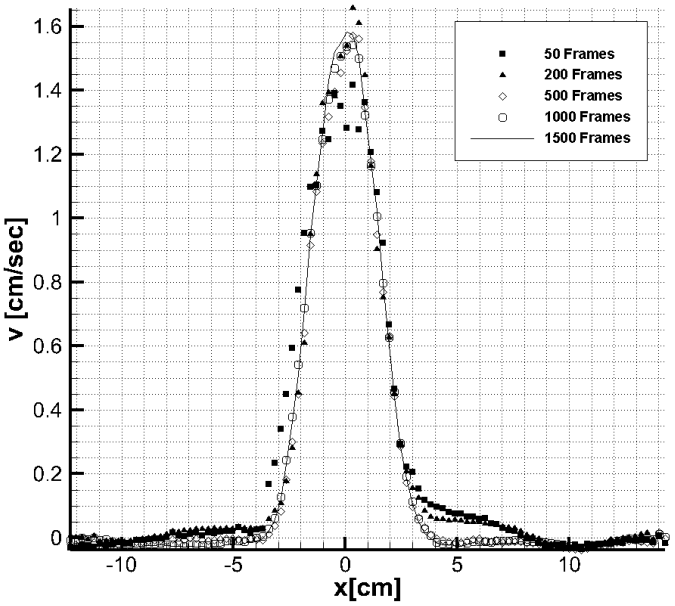

Figure 44. The sensitivity analysis at 9 cm from the pipe outlet for test 2.

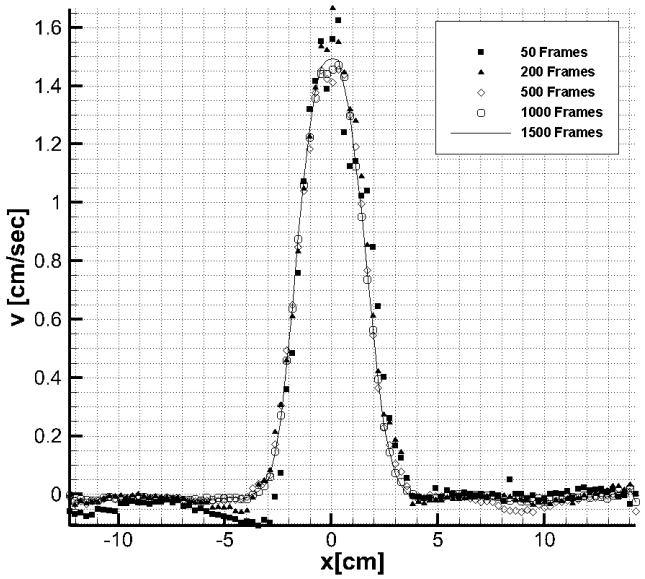

Figure 45. The sensitivity analysis at 9 cm from the pipe outlet for test 3.

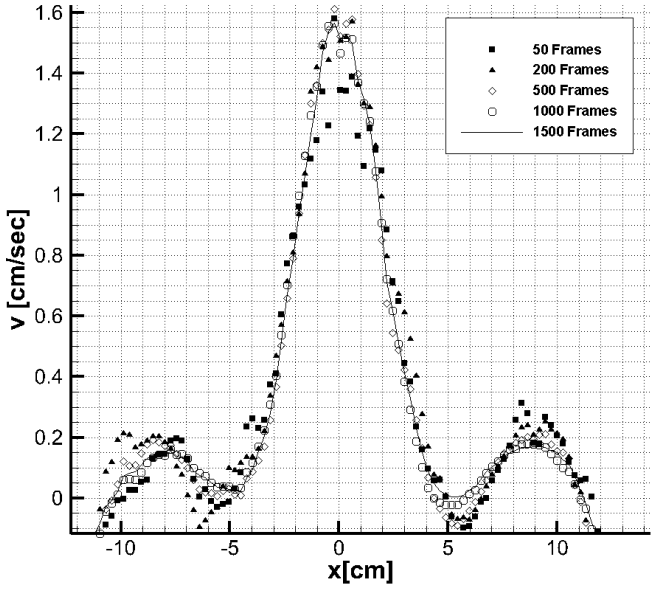

Figure 46. The sensitivity analysis at 15 cm from the pipe outlet for test 1.

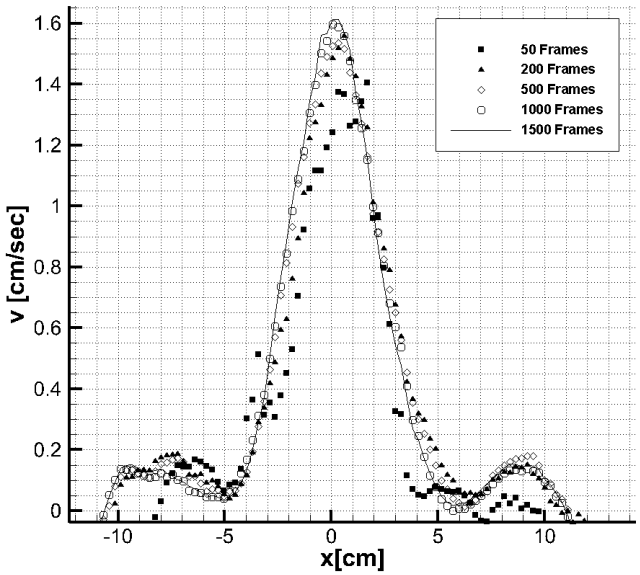

Figure 47. The sensitivity analysis at 15 cm from the pipe outlet for test 2.

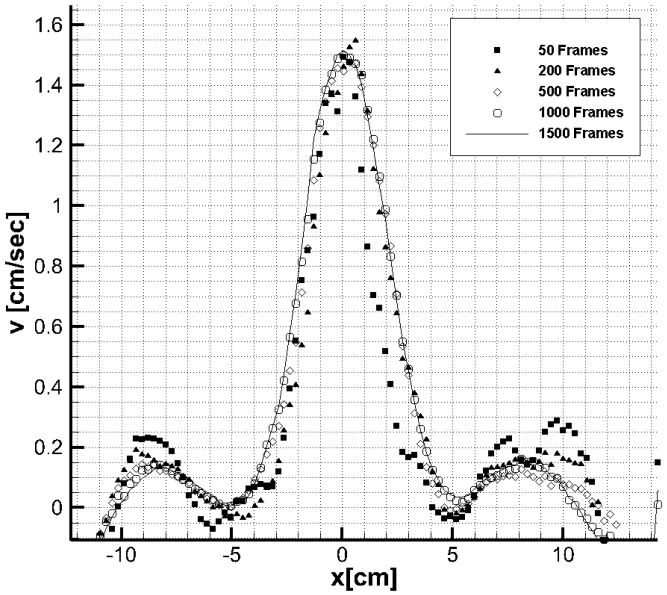

Figure 48. The sensitivity analysis at 15 cm from the pipe outlet for test 3.

IV.3.3. Repeatability

In any experimental research, the accuracy and precision of the result is critical. In this experiment, the conditions of one test may differ another, even when using the same procedure. For example, cooling temperature may not be exactly the same all the time, room temperature may vary with time, and uncertainty of other measurement devices may affect results. Repeatability of different tests could reduce the error of the out by calculating the average of all the tests. This was done by using ensemble average equation for all the three tests.

$$v_{avg} = \frac{1}{n}\sum_{n=1}^{3} v_n \tag{IV.4}$$

Where v_n is the velocity profile for test number n, and n is the test number.

After the average was calculated, an uncertainty should be included. This was done by calculated the standard deviation v_{rms}, or the root mean square RMS, of the three tests.

$$v_{rms} = \sqrt{\frac{\sum_{n=1}^{3}\left(v_n - v_{avg}\right)^2}{n}} \tag{IV.5}$$

Also, turbulent intensity is calculated to provide an overview of how the plume is acting at different levels of the upper plenum. The turbulent intensity is calculated as:

$$I = \frac{v_{rms}}{v_{avg}} \tag{IV.6}$$

Matlab code was used to calculate averages standard deviations of the three tests and then the output was plotted for the three different lines, y = 3, 9 and 15 cm, as shown in Figure 49, 50Figure 50 and 51 . At 3 cm, the uncertainty at the center of the pipe ranges from 7 to 14%. This area also has a high turbulent intensity, which explains why the *v* standard deviation is high.

At 9 cm, *v* standard deviation ranges from 4 to 6% and there is medium turbulent intensity, with the flow becoming more stable and with fewer fluctuations. Finally at 15 cm, the flow is more stable and as a result error decreases to a range of 1 to 3%. The flow here has low turbulent intensity, which why the velocity profile for all three tests at this area have less error and are more similar.

Figure 52 show standard deviation for all Y-elevations of the average velocity of the three tests taken at the centerline of the pipe. The RMS is highest near the output of the pipe at approximately 0.30. At 2 cm a dip in error occurs, with the RMS going to approximately 0.02. The error increases after 2 cm, but starts to decrease again at 4 cm, where it is 0.175. After that is the area of the glue part, where data are missing. After the glue part, the flow estimates have an error from 0.07 to 0.12. Flow becomes more stable at approximately 12 cm with error reduced to 0.02. From 12 cm until the edge of the upper plenum, the flow continues to show slight instability.

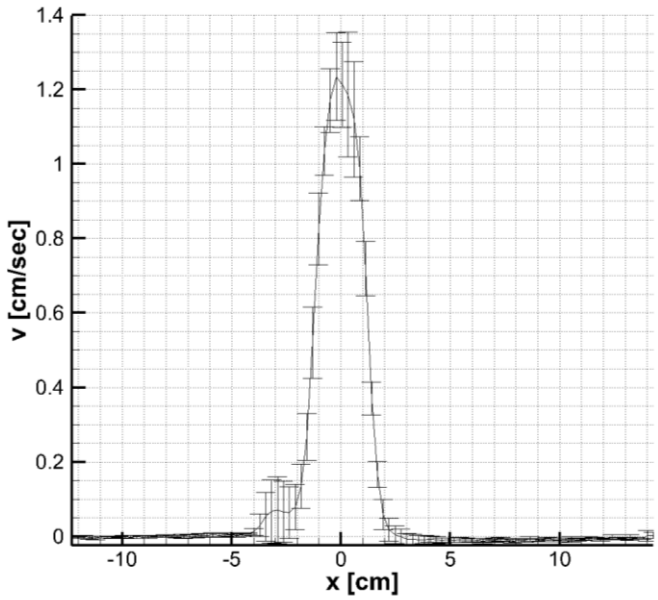

Figure 49. The ensemble average of y-velocity with the v_{rms} for all tests at 3cm

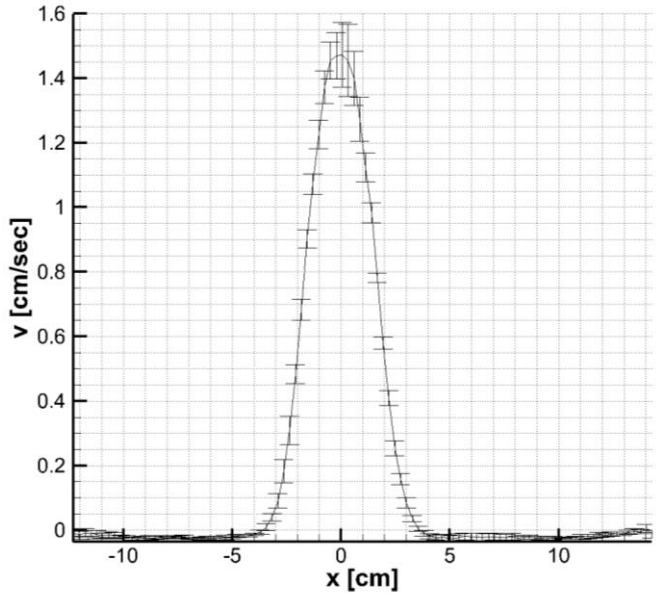

Figure 50. The ensemble average of y-velocity with the v_{rms} for all Tests at 9cm

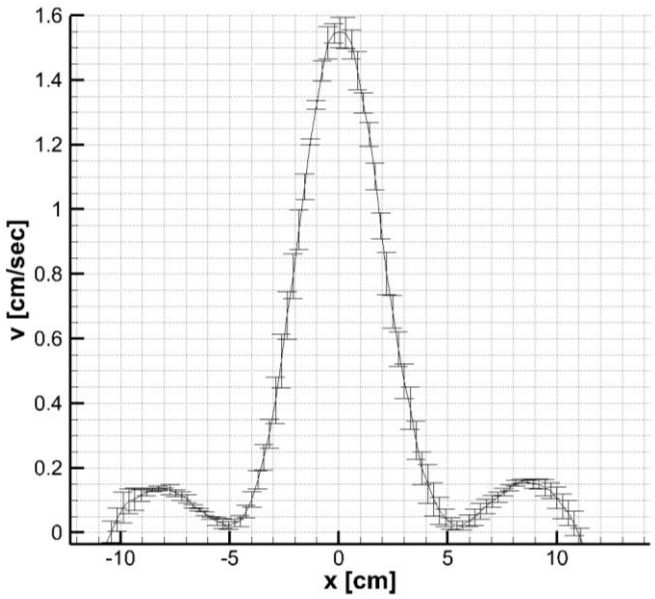

Figure 51. The ensemble average of y-velocity with the v_{rms} for all Tests at 15cm

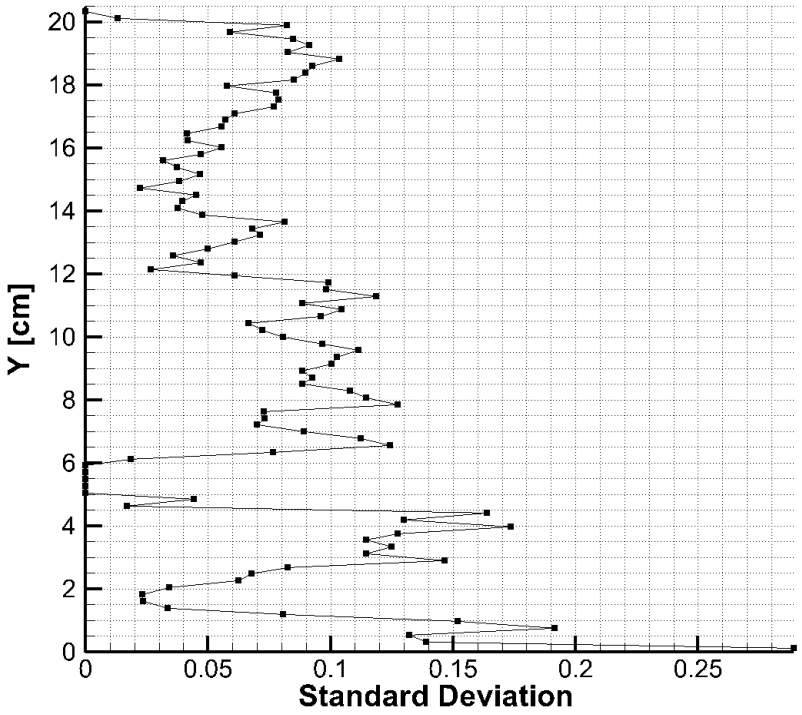

Figure 52. Standard deviation for all y-elevation for the average tests at the centerline of the pipe.

The uncertainty of PTV depends mainly on its ability to find the centroid of the particles; finding and tracking the particle centroid is critical. Based on previous research on measuring flow using PTV, it is assumed in this experiment that the uncertainty of PTV is less than 0.1 px/Dt [23]. In addition, the standard deviation v_{rms} could be considered as an uncertainty of the test. As mentioned above, it ranges from 1 to 14%, which is less than ideal, suggesting that repetition of more tests could reduce the uncertainty of the experiment.

IV.3.4. Validation

After averaging the output and using repeatability to confirm the 1500 pairs of images are enough to reach a steady state average, the data are trivial if not validated. In this experiment, the data are validated by comparing it to benchmark data.

The fluid is laminar before entering the upper plume, and it is inside the upper plenum that the fluid starts to become turbulent. To account for the turbulent fluctuations, Reynolds stress can be used to give an overview of the stress tensor in the system. Reynolds stress is calculated as:

$$R_{ij} = \overline{u'_\iota u'_J} \tag{IV.7}$$

Figure 53 shows the experimental Reynolds stress at 3 cm from the output of the pipe. Figure 54 shows the Reynolds stress from Hussein [24], who studied velocity measurements in a high Reynolds number momentum conserving, axisymmetric,

turbulent jet [24]. It should be observed that Reynolds stress starts to decay at the edge of the plume; Reynolds stress become to be more self-similar [25].

The <*uu*> and <*vv*> have similar pattern to those in the Hussein paper [24]. However, <*uv*> begins similarly to Hussein's results, then goes below zero, before return to the same pattern as in Hussein's paper. Turbulent intensity, reveals a similar pattern. The profile here starts to increase as the Reynolds stress decays (Figure 55 and 56) [25].

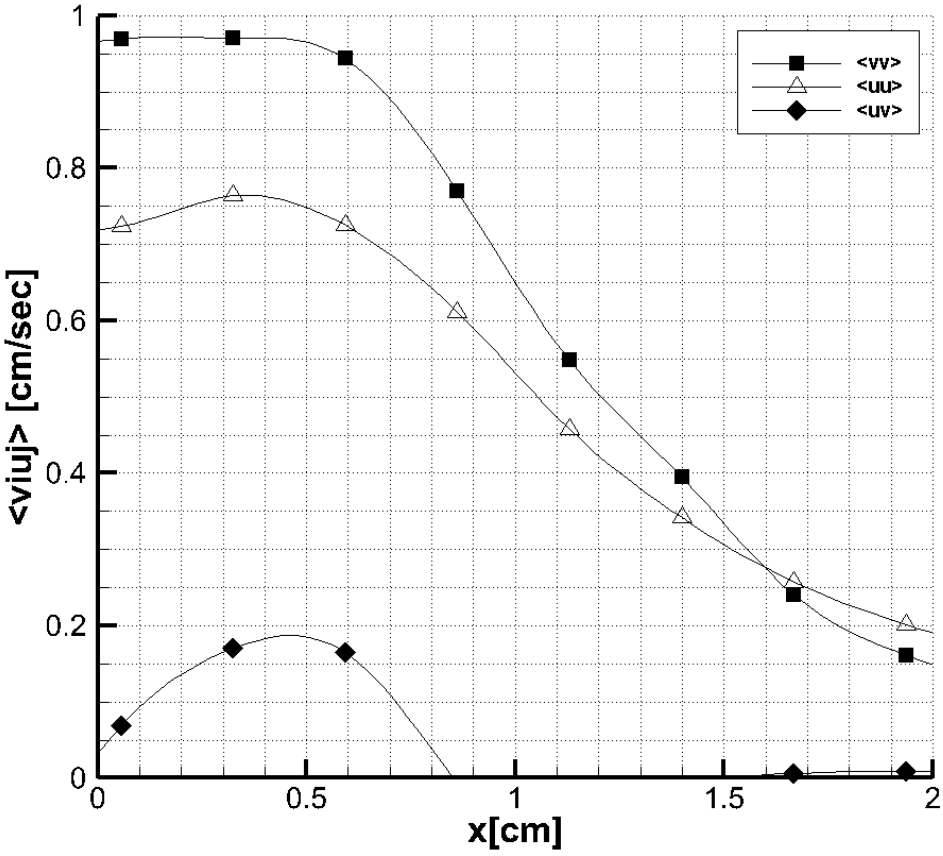

Figure 53. Reynolds stress profile at three y-lines extracted.

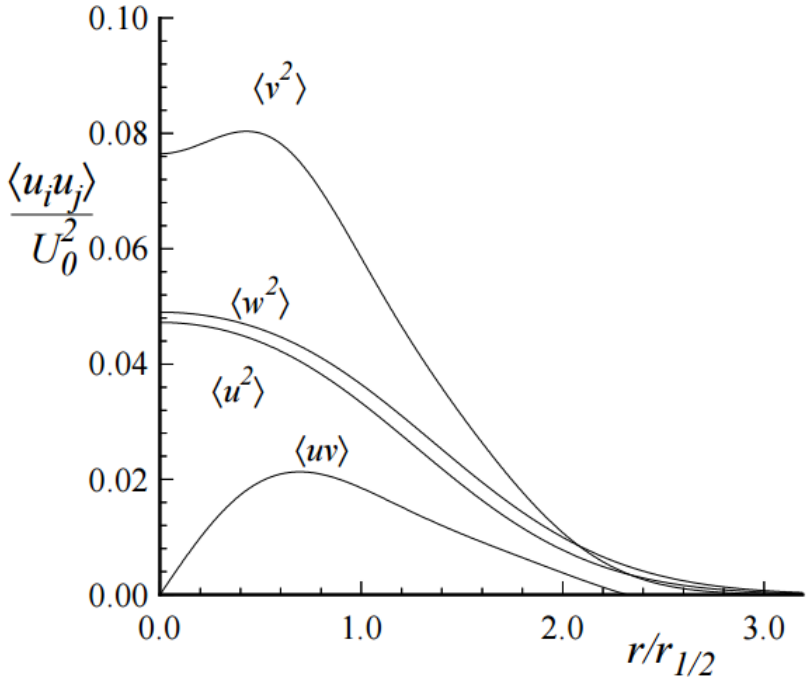

Figure 54. Reynolds stress profile from Hussein experiment.

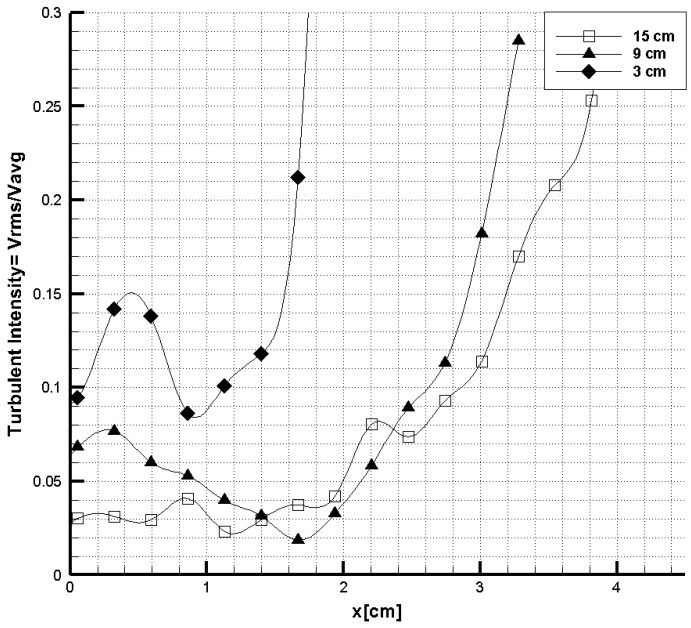

Figure 55. Turbulent intensity profiles at three y-lines extracted.

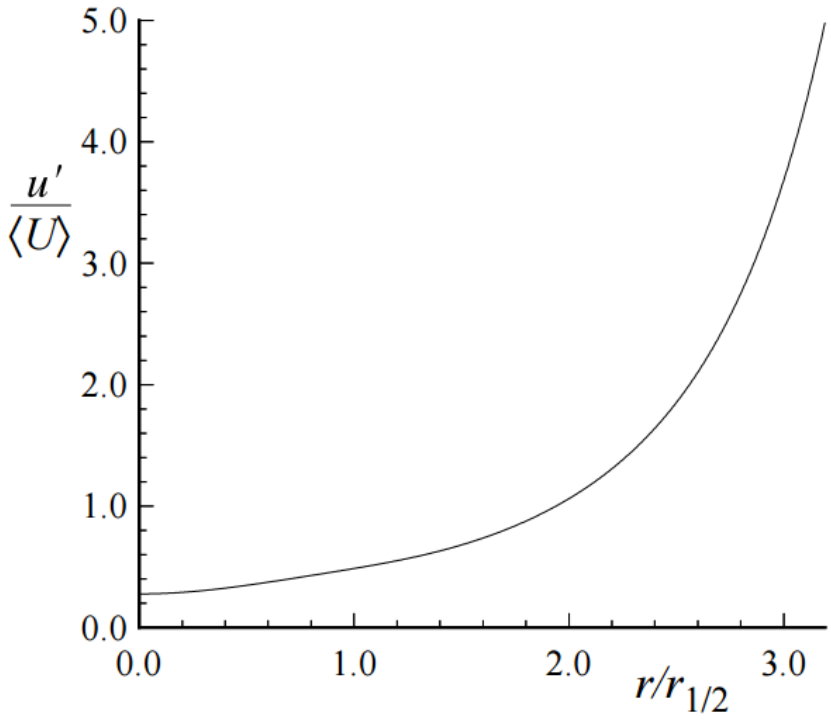

Figure 56. Turbulent intensity profile from Hussein experiment.

CHAPTER V

CONCLUSION AND FUTURE WORK

V.1. Conclusion

A $1/16^{th}$ scaled upper plenum of VHTR was designed and assembled. The goal of this test facility was to study flow at the upper plenum of a VHTR during a DCC accident scenario. After a preliminary test of the facility, it was reassembled to fix some leaks and thermocouples that were not calibrated properly. In addition, the ultrasound flow meter was re-calibrated using the electromagnetic flow meter to reduce measurement error in the system. A high speed camera was mounted in a fixed position. The laser was tested and its power and frequency were chosen. Fluorescent orange particles with 1.002 g/cc density were selected as seed source.

The procedure of the experiment and all instruments used are explained in detail in this thesis. Multiple tests were done and evaluated. Three tests were chosen to analyze flow. The flow was driven by natural convection due to heat in the core, so that flow from the pipe was considered to be a plume rather than a jet. The flow began as a laminar flow, but became turbulent as it entered the upper plenum.

Visual basic code was written to process image pairs. Image vectors were first filtered, then Matlab code was used to combine all output and tecplot software used to visual flow and the velocity counter.

A total of 3000 images (1500 image pairs) were used to quantify the velocity field at the upper plenum. A sensitivity analysis confirmed that1500 frames were

sufficient to precisely estimate flow. Subsequently, three (3, 9, and 15 cm) Y-lines from the pipe output were extracted to consider the output differences between 50 to 1500 frames. The flow reaches the steady state with 1000 frames or more.

The average velocity field in the three different tests calculated and the standard deviation error that accrued used to assess repeatability. The error was varied, from 1 to 14%, depending on Y-elevation. The error decreased as the flow moved farther from the output pipe. In addition, turbulent intensity was calculated and found to be high near the output.

Reynolds stress and turbulent intensity were used to validate the data by comparing it with benchmark data. The experimental data gave the same pattern as the benchmark data.

V.2. Future Work

The aim of this study was to understand the behavior of the flow at the upper plenum of a reactor under a DCC accident scenario by using PTV technique. Future work is needed to investigate different techniques for measuring flow technique and to study the flow with more than one pipe to provide benchmark data. Laser Doppler velocimetry (LDV) is another technique to study the velocity of the system. It could be applied in this experiment to allow comparison among PTV, PIV and LDV. Computational fluid dynamics (CFD) is needed to validate the data and it can be then applied to the real VHTR. Finally, as the test facility is able to run other types of accident scenario, investigating PCC and other accident scenarios can help improve our understanding of behavior of the flow at the upper plenum.

REFERENCES

[1] "World Energy Outlook 2014," International Energy Agency, Paris, France, 2014.

[2] "Nuclear Power in the World Today," World Nuclear Association, 2015.

[3] N. R. Commission, "Boiling Water Reactor (BWR) Systems," NRC, 2015.

[4] N. R. Commission, "Pressurized Water Reactor (PWR) Systems," NRC, 2015.

[5] "The ABWR Plant General Description," General Electric, December 2006.

[6] "Generations of nuclear technology," European Commission, Research & Innovation, 2014.

[7] S. K. a. J. N. Doug Chapin, "The Very High Temperature Reactor: A Technical Summary," MPR Associates, Inc , Alexandria, VA, 2004.

[8] "A Technology Roadmap for Generation IV Nuclear Energy Systems," U.S. DOE Nuclear Energy Research Advisory Committee and the Generation IV International Forum, December 2002.

[9] H. Haque, W. Feltes, G. Brinkmann, "Thermal response of a modular high temperature reactor during passive cooldown under pressurized and depressurized conditions," *Nuclear Engineering and Design*, vol. 236, pp. 475-484, 2006.

[10] K. G. C. ,. a. R. R. S. Glenn E. McCreery, "Scaled Experimental Modeling of VHTR Plenum Flows," in *International Conference on Nuclear Energy (ICONE 15)*, Nagoya, Japan, 2007.

[11] D. Tritton, Physical Fluid Dynamic, New York, USA: Van Nostrand Reinhold, 1997.

[12] B. M. King, Natural Circulation Scaling of a Pressurized Conduction Cooldown Event in the Upper Plenum of the Modular High Temperature Gas Reactor, Oregon State University, 2013.

[13] N. B. L., "Scaling Analysis for the Pebble Bed of the Very High Temperature Gas-cooled Reactor Thermal Hydraulic Test Facility," Oregon State University, 2009.

[14] Kyle L. McVay, Jae-Hyung Park, Saya Lee, Yassin A. Hassan, N.K. Anand, "Preliminary tests of particle image velocimetry for the upper plenum of a scaled model of a very high temperature gas cooled reactor," *Progress in Nuclear Energy,* vol. 83, pp. 305-317, August 2015.

[15] M. Jahanmiri, "Particle Image Velocimetry: Fundamental and Its Applications," Chalmers University of Technology, Goteborg, 2011.

[16] M. Raffel, C. Willert, S. Wereley, J. Kompenhhans , Particle Image Velocimetry, Heidelberg: Springer, 2007.

[17] R. J. Adrian, "Particles-Imaging Techniques For Exprerimental Fluid Mechanics," in *Annual Review of Fluid Mechanics,* 1991, pp. 261-304.

[18] D. Dynamics, "Measurement Principles of PIV," http://www.dantecdynamics.com/, 2014.

[19] Sijie Fu, Pascal-Henry Biwolé, Christian Mathis, "A Comparative Study of Particle Image Velocimetry (PIV) and Particle Tracking Velocimetry (PTV) for Airflow

Measurement," *International Journal of Mechanical, Aerospace, Industrial, Mechatronic and Manufacturing Engineering*, vol. 9, no. 1, 2015.

[20] R. J. Adrian, "Particle-Imaging Techniques for Experimental Fluid Mechanics," *Annual Review of Fluid Mechanics*, vol. 23, no. 1, pp. 261-304, Jan. 1991.

[21] "Thermocouple Info," 2015. [Online]. Available: http://www.thermocoupleinfo.com/index.htm.

[22] C.E. Estrada-Perez, Y.A. Hassan, "PTV experiments of subcooled boiling flow through a vertical rectangular channel," *International Journal of Multiphase Flow*, vol. 36, no. 9, pp. 691-706, 2010.

[23] C.E. Estrada Perez, Junsoo Yoo, Yassian Hassan, "Feasibility investigation of experimental visualization techniques to study subcooled boiling flow," *International Journal of Multiphase Flow*, vol. 73, pp. 17-33, 2015.

[24] Hussein J. Hussein, Steven P. Capp, Willam K. George, "Velocity measurements in a high-Reynolds-number, momentum-conserving, axisymmetric, turbulent jet," *Journal of Fluid Mechanics*, vol. 258, pp. 31-75, 1994.

[25] S. B. Pope, Turbulent Flows, United Kingdom: The MPG Books Group, 2000.

[26] K. Mcvay, "Experimental Design and Flow Visualization for the Upper Plenum of a Very High Temerature Gas Cooled for Computer Fluid Dynamics Validation," Texas A&M University, College Station, 2014.